Applied Thermal Engineering 255 (2024) 123943

Contents lists available at ScienceDirect

Applied Thermal Engineering

journal homepage: www.elsevier.com/locate/apthermeng

Research Paper

Small scale CO_2 based trigeneration plants in heat recovery applications: A case study for residential sector in northern Italy

Mattia Baiguini [a,b,*], Michele Doninelli [a], Ettore Morosini [c], Dario Alfani [c], Gioele Di Marcoberardino [a], Paolo Giulio Iora [a], Giampaolo Manzolini [c], Costante Mario Invernizzi [a], Marco Astolfi [c]

[a] Università degli studi di Brescia, Dipartimento di ingegneria meccanica e industriale, Via Branze 38, 25123 Brescia, Italy
[b] Scuola Universitaria Superiore IUSS Pavia, Piazza Vittoria 15, Pavia, 27100, Italy
[c] Politecnico di Milano, Dipartimento di energia, Via Lambruschini 4a, 20156 Milano, Italy

ARTICLE INFO

Keywords:
Trigeneration
Adsorption chillers
Heat recovery
pure CO_2 and mixtures
Techno-economic analysis

ABSTRACT

This study investigates the potential of trigeneration systems utilizing CO_2-based power cycles to harness high-temperature excess heat. Various CO_2-based cycles are proposed, comprising pure CO_2 and CO_2-mixture, emphasizing integration into district heating and cooling networks. Given the non-isothermal heat rejection of CO_2-based cycles, performance maps for absorption chillers at different thermal levels and temperature drop of the heat source are generated. These maps are beneficial not only for the current study but also for generic applications. Various cycle layouts are studied, employing strategies to maximize overall electrical efficiency, electrical power output, or thermal production, starting from available high-grade heat above 500 °C. Depending on the specific cycle layout and strategy, the optimal cycle-thermal user coupling is evaluated. The economic and environmental viability of the proposed solution is evaluated in comparison to an existing case-study in northern Italy where the exhaust gases of 10 MW_{el} gas turbines are currently exploited for district heating purposes and centralized vapour-compression chillers meet the residential cooling demand. Compared to the case-study, the adoption of a simple recuperative CO_2-mixture bottoming cycle, at a minimum cycle temperature of 70 °C, allows not only a primary energy saving of 16 % but also an 8 % reduction of levelized cost of electricity.

1. Introduction

Over the last decades, the demand and production of thermal power for space heating and cooling applications grew significantly: the International Energy Agency reports that, from 1990 to 2016, the space cooling demand has tripled, and it is mainly provided by air conditioning systems, consuming 2000 TWh of electricity per year worldwide [1]. Moreover, fossil fuels account for the 64 % of the primary energy used for space heating, with natural gas covering 42 % of the share (corresponding to around 760 billion Nm^3 in 2021) [2].

The heat rejected by industrial processes can be a potential source to cover the demand for space heating and cooling, even in cases where it is already exploited for electricity production, in a bottoming thermal recovery system. In this scenario, poly-generation plants are crucial not only to achieve high overall efficiency, but also to save primary energy and provide flexible operation. Cogeneration plants, or combined heat and power (CHP) plants, represent a consolidated technology, where electricity and hot water are produced as outputs. In principle, a CHP plant can adopt different layouts [3–5], such as a gas turbine coupled by a heat recovery steam generator (HRSG), a steam Rankine cycle or an Organic Rankine Cycle (ORC). In case of steam and organic Rankine cycles, the production of heat for thermal user is obtained penalizing the electric production: in order to match the temperature level of district heating (DH) systems, typically in the 65–90 °C range [6], the expansion of the turbine is either limited in the so called backpressure configuration or part of the expanded flow is bled from the turbine, thus decreasing both electric efficiency and electric power. Another possibility of poly-generation plants is represented by combined cooling, heating and power generation (CCHP) systems, which can simultaneously provide three different outputs: electricity, hot water and chilled water for a DH and district cooling (DC) networks.

ORCs are nowadays the most used technology for waste heat recovery from industrial processes with temperatures below 500 °C or

* Corresponding author at: Università degli studi di Brescia, Dipartimento di ingegneria meccanica e industriale, Via Branze 38, 25123 Brescia, Italy.
E-mail address: mattia.baiguini@unibs.it (M. Baiguini).

https://doi.org/10.1016/j.applthermaleng.2024.123943
Received 31 January 2024; Received in revised form 12 July 2024; Accepted 12 July 2024
Available online 14 July 2024

Nomenclature

Acronyms

AC	Absorption Chiller
CAPEX	Capital Expenditure [$]
CCHP	Combined Cooling Heat and Power
CHP	Combined Heat and Power
COP	Coefficient Of Performance [-]
CS	Cascade cycle
DC	District Cooling
DEAC	Double Effect Absorption Chiller
DH	District Heating
EE	Electric Energy
EEC	Efficiency Energy Certificate [$/toe]
ELECNRTL	Electrolyte-NRTL
HRecU	Heat Recovery Unit
HRejU	Heat Rejection Unit
HRSG	Heat Recovery Steam Generator
HTF	Heat Transfer Fluid
LCOE	Levelized Cost of Electricity [$/MWh]
LHV	Lower Heating Value [MJ/kg]
MPP	Maximum Power Production
MEE	Maximum Electric Efficiency
MTR	Maximum Thermal Recovery
OPEX	Operation & Maintenance [$/y]
PES	Primary Energy Saving [-]
PHE	Primary Heat Exchanger
SEAC	Single Effect Absorption Chiller
SR	Simple Recuperative
TIT	Turbine Inlet Temperature [°C]

Roman and Greek letter

E	Energy, [MWh]
P	Pressure [bar]
$\dot{Q}$	Thermal power, [MW]
T	Temperature [°C]
$\dot{W}$	Mechanical/electric Power [MW]
p	Selling price [$/MWh$_{el}$]
ΔT	Temperature difference [°C]
η	Efficiency [-]
χ	Recovery factor [-]

Chemical formula

CO_2	Carbon Dioxide
C_6F_6	Hexafluorobenzene
H_2O	Water
$LiBr$	Lithium Bromide

Subscript

c	compression
cond	condensation
eva	evaporation
gb	gas boiler
grid	Electric grid
hs	heat sourse
m	motor
min	minimum
ref	reference
tot	total
t	turbine

even higher [7] and from small gas turbines (below 10 MW_{el}) [8]. Nevertheless, in recent years, pure carbon dioxide (CO_2) [9] and CO_2-based mixtures [10,11] power cycles have been proposed as an alternative technology to ORC (and steam cycles in large size applications) thanks to the high performance, the promising fluid thermal stability and the compactness of plant components [12]. In particular pure and CO_2 mixtures have been recently investigated in several European H2020 funded projects as in SCARABEUS, DESOLINATION, CO_2OL-HEAT, SCO_2FLEX and SOLARSCO_2OL, for different applications. The concept of poly-generation is known in the literature regarding both power cycle or fuel cells [13–15]. Moreover Bellos et al have been considered poly-generation system adopting CO_2 power block [16]. The authors reported few examples: the systems adopting concentrated solar power as primary energy source can achieve an overall efficiency in the range of 40 % to 160 % to mainly produce electricity, heating and cooling, and in some cases also hydrogen [16]. On the other hand, systems using biomass or a geothermal source, reach an efficiency of 60 % to produce the same outputs [16]. These plants are typically composed by a topping power cycle and a bottoming system like an ORC, an HRSG, an absorption chiller and an electrolyser.

Another study conducted by Moroz et al. [17], focusing on a pure CO_2 CHP plant powered by fossil fuel combustion with a primary heat source of 790 MW, shows an electricity efficiency between 17 % and 40 % and heat utilization factor from 38 % to 95 % depending on the architecture of the plant. Considering then other literature works with complex systems including a chemical loop reactor [18], the net power efficiency of the CO_2 power block is found at around 40–43 % and the thermal efficiency is up to 40 %. Considering instead only CO_2 based CCHP system, Yang et al. [19] conducted a literature review showing that this kind of plants could reach overall CCHP efficiencies up to 75 %. In the same work the authors proposed a novel system adopting the recompression CO_2 cycle obtaining an overall efficiency up to 70 % and 55 % in combined heating and power and in combined cooling and power mode, respectively. As final example, Zhang et al [20] proposed a CO_2 Brayton cycle coupled with an ORC and a desalination process achieving an 26.16 % as overall efficiency.

Focusing on CHP systems based on CO_2 mixtures power cycles, a previous literature publication was proposed by the authors of this work [21], assuming as hot source the exhaust gases from an industrial process at 450 °C: the results underlined the advantages of coupling CO_2-based power cycles with a high (180 °C) and a low temperature (100 °C) thermal user, in a cogenerate perspective. While with a conventional pure fluid power cycle, the heat rejection (HR) is dominated by an isothermal condensation of the working fluid, in CO_2 based power cycles the temperature level of the heat rejection is variable and it can be exploited in a more effective way, as shown in Fig. 1.

Considering pure CO_2 cycles, the temperature level in the HR process is higher if compared to ORC technology and it ranges from around 100–110 °C to minimum cycle temperature [21,22]. Additionally, using CO_2 mixtures allows having not-isothermal conditions during the heat rejection even when considering condensing cycles, thanks to the exploitation of the temperature glide which permits to optimize the temperature match between the working fluid and the thermal user. Considering the above mentioned literature work of Morosini et al. [21], a waste heat recovery case with a thermal source in the range of 15 to 30 MW, the authors found that the electric power produced from the bottoming CO_2-based CHP systems can be around 13–20 % of the thermal input, while the recovered thermal power can be 66–83 % of the thermal input (10–25 MW_{th}): 40 % in the 105–200 °C range for industrial uses and 60 % for district heating [21]. Another example of CHP plant based on CO_2 mixtures is presented by Doninelli et al. [23] where the heat rejection of the power block is exploited to produce freshwater from seawater with a thermally-driven desalination system, obtaining a cogeneration efficiency close to 100 % and lowering the cost of

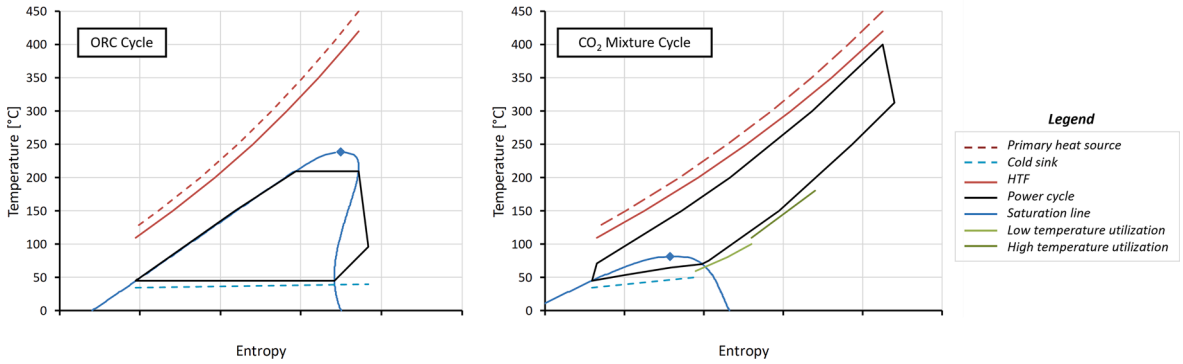

Fig. 1. Temperature vs Entropy for ORC power cycle (left). Temperature vs Entropy and heat recovery characterization of the transcritical CO_2-based power cycle (cascade layout) working fluid for CCHP applications (right) [21]. The rhombus dot refers to the critical point.

freshwater production with respect to more conventional technologies.

This work investigates the trigeneration potential of both pure CO_2 and CO_2-mixtures power cycles for heat recovery applications. It begins by modelling the production of cold thermal power for a district cooling network, including a detailed analysis (Section 2.3) of absorption chiller (AC) systems to estimate their coefficient of performance (COP) under various heat source conditions. Next, different configurations of CO_2-based power cycles are explored to identify the most effective coupling with district heating and cooling networks. The study includes a case study focusing on revamping an existing CCHP plant in Milan, Italy, involving small-scale gas turbines, HRSG, and compression chillers. The proposed solution utilizes heat rejected from the CO_2 power block and low-temperature exhaust gases to produce hot water for district heating in winter and chilled water for district cooling in summer, reducing the need for electric consumption by compression chillers. Finally, a techno-economic analysis compares the original system with the proposed solution to minimize electricity production costs, while also calculating the avoided emissions to assess the environmental impact of the retrofit.

Considering the provided literature review of CO_2-based CHP and CCHP systems, the novelty of this work lies primarily in the analysis of CO_2 mixture-based CCHP plants. Typically, CO_2 mixture-based power plants are proposed for large-scale applications, such as concentrated solar power plants, whereas this work focuses on heat recovery coupled with residential sector district heating and cooling. Under this perspective, the cold thermal load is provided directly as a byproduct of the power cycle, without any auxiliary electric consumption, by stressing the promising coupling between the power and the refrigeration section from the point of view of the temperature range at the cycle heat rejection unit. Additionally, it introduces performance maps and a polynomial regression equation for estimating the COP of absorption chillers under various heat source conditions, based on typical machinery assumptions. Supplementary Materials include also a code for convenience. Furthermore, the paper discusses optimized matching between district heating and cooling systems and the CCHP plant, providing valuable insights for future research in the field.

2. Methodology

The study explores a CCHP plant featuring two gas turbines and a CO2-based bottoming power block, replacing a HRSG for hot water production. Heat for the DH and DC networks in the proposed setup is collected from the cycle's heat rejection and flue gases at the primary heat exchanger (PHE) outlet. Chilled water is produced using absorption chillers with various layouts. Modelling accounts for literature-derived assumptions and parameters, aiming to compute system performance, including chiller COP and cycle efficiency under different conditions. The results from the modelled absorption chillers are applicable to any hot source category, expanding the study's relevance and impact. The commercial software Aspen Plus® V12 [24] is utilized throughout the study to simulate component and plant performance, employing chemical and physical models for accurate representation.

2.1. Case study

An existing trigeneration power plant is selected as case study, located in the city of Milan, Italy [25], with a district heating and cooling network currently in operation connecting domestic users [25]: a simplified flow diagram of the current configuration of the CCHP plant is shown in Fig. 2 (left).

The electric power is generated by two Taurus 60S-7801 5 MWel gas turbines by Solar Turbine [26], serving both self-consumption and selling electricity to the national grid. Each turbine runs on natural gas, providing 17 MW of input thermal power (on LHV basis) at standard conditions, with an electric efficiency of around 29 %. The expander outlet temperature is 510 °C, and the total flue gas mass flow rate is 43.22 kg/s for both turbines. Hot water production is facilitated by an HRSG with a capacity of 16 MWth installed at the turbine outlet, supplemented by additional gas boilers, resulting in an overall DH capacity of 87 MWth. The plant currently operates with four compression chillers (three operational and one backup), each capable of producing 2.5 MWth (7.5 MWth cold thermal load at design conditions). DH water is supplied at 95 °C with a return temperature of 60 °C [27], and the chilled water temperature ranges from 6 °C to 12 °C [6]. To ensure a fair comparison between the existing and retrofitted plant configurations, certain boundary conditions regarding the turbines, HRSG, and operational chillers are detailed in Table 1, serving as the reference case for analysis.

On the other hand, the proposed retrofitted solution includes the CO_2-based power cycle for additional electricity production, replacing the HRSG and the compressor chillers as shown in Fig. 2 (right). In this configuration, the heat rejected by the bottoming power cycle, together with the fraction of heat, which is not recovered from the flue gases, can be exploited to produce both hot and/or chilled water according to the available temperature levels.

2.2. Trigeneration power cycle

The simulations of the new bottoming power cycles in the proposed retrofit are based on a flue gas stack temperature of 120 °C, enabling recovery of 18.33 MW_{th} of available thermal power at full load. To maintain simplicity and considering flue gas composition, an intermediate heat transfer fluid (HTF) loop isn't introduced, and a minimum pinch temperature difference of 30 °C is assumed in the primary heat exchanger (PHE) between exhaust gases and the working fluid.

The power block configurations adopted for this heat recovery application are the simple recuperative (SR) and the cascade (CS) cycle, which was already suggested in a previous work [21], as it features a heat rejection at relatively high temperatures (Fig. 1). In this work, the

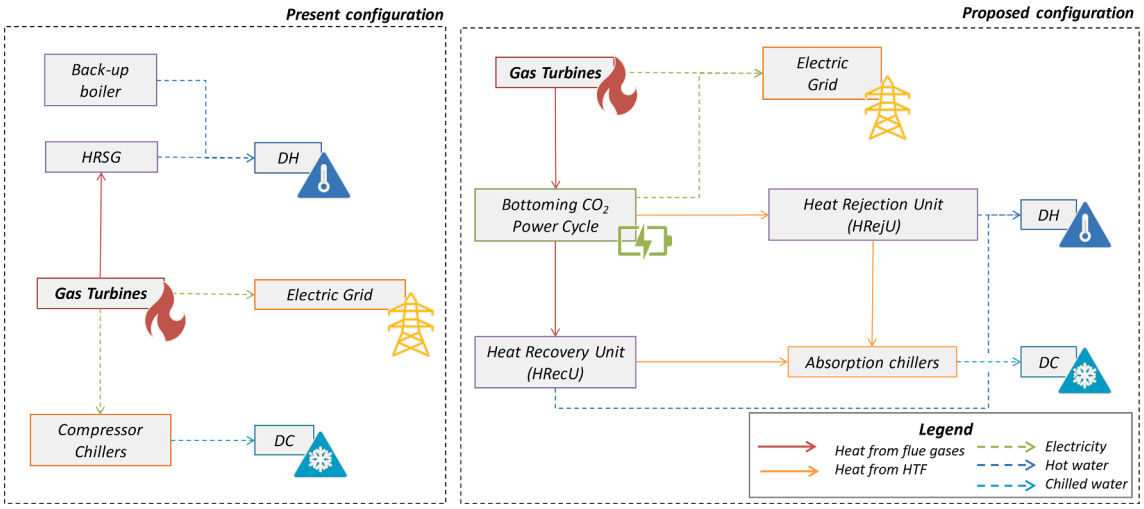

Fig. 2. CCHP power plant. Present layout (left) and proposed layout (right).

Table 1
Nominal capacity of the existing CCHP power plant components.

Components	Overall power produced
Gas turbines (electric power)	10 MW_{el}
HRSG (hot thermal power)	16 MW_{th}
Compression chillers (cold thermal power)	7.5 MW_{th}

layout for the cascade cycle is proposed in two configurations (Fig. 3 – upper) that differs in the internal heat recuperation process, with three distinct design criteria: i) the maximization of the thermal recovery from the exhaust gases (MTR), to ensure a complete exploitation of the heat source from the power plant, ii) the maximization of the electric power production (MPP) and iii) the maximization of the electric efficiency (MEE). Each cycle configuration is investigated with both pure CO_2 in a supercritical cycle and with a CO_2-mixture in transcritical condition.

The MTR configuration adopts just one recuperator which exploits the residual heat of the main fraction of the working fluid at the high temperature turbine outlet to heat up the remaining working fluid fraction which is then expanded in the low temperature turbine. As a result, the heat introduction process starts right after the compressor (for pure CO_2 cycle) or the pump (in case of CO_2-mixtures), allowing for a complete cooling of the heat source and leading to a unitary value of the heat source recovery factor ($\chi = \dot{Q}_{PHE}/\dot{Q}_{fg}$ where $\dot{Q}_{PHE}$ is the input thermal power in the PHE). The heat rejected by the cycle is recovered in the heat rejection unit (*HRejU),* divided in a high and a low temperature, by heating up two different HTF loops based on pressurized water (Fig. 3 – top left). On the contrary MPP and MEE cycles adopt an additional recuperator (*REC LT*) to preheat the high temperature working fluid loop before the main heat introduction process by cooling down the hot working fluid at the outlet of the low temperature turbine. In this case the internal heat recovery is improved, leading to a higher cycle thermodynamic efficiency at the expense of a lower heat source recovery factor. As a result, the heat source is not fully exploited: for this reason, it is further cooled down to the stack temperature in an additional heat recovery unit (*HRecU*) (Fig. 3 – upper right).

In the analysis to revamp the current trigeneration plant in Milan, the calculations align with the temperature range of the existing DH and DC networks. To achieve this, an intermediate loop of hot pressurized water is introduced to prevent direct heat transfer between the cycle's working fluid and both the district heating water and the absorption chiller working fluid, as illustrated in Fig. 3. The temperature range of the intermediate loop must be compatible with the heat source and the user, with a minimum 5 °C pinch point in each heat exchanger. Further details on matching the HRejU and HRecU with the power block and thermal demand are discussed in Section 3.3.

The SR analysis focuses solely on using CO_2 mixture and the maximum electrical efficiency (MEE) design approach. The cycle's recuperative nature allows for significantly high efficiency, while the reduced number of components lowers capital costs compared to the CS cycle [28]. Additionally, adopting the SR configuration with a CO_2 mixture outperforms the recompressed layout for pure CO_2, as the mixture achieves more balanced heat capacities in the recuperator without needing additional recompression typically used in CO_2 cycles [28].

During modelling, a sensitivity analysis varies the cycle's minimum temperature (T_{min}) between 50 °C and 70 °C with a 5 °C step. Ambient air serves as a cold sink for the fraction of rejected thermal power not used for heating or cooling, specifically below 65 °C. For each of the three cycle design criteria (MTR, MPP, MEE), and for both pure CO_2 and blended CO_2 (a total of 35 combinations), the power plant is optimized. This optimization maximizes electric power for MTR and MPP architectures, balancing heat recovery and cycle thermodynamic efficiency (guaranteeing $\chi = 1$ for MTR), and maximizes electric efficiency for the MEE criterion.

In the optimization procedure, the following design parameters are varied: i) the cycle maximum temperature, ii) the cycle minimum pressure for CO_2 cycles (while in CO_2 mixture it depends in the molar dopant fraction being set the cycle minimum temperature) and iii) the split fraction after the pump/compressor (only for CS cycles). As already proposed in literature, using CO_2-mixtures in transcritical configurations, hence operating the compression in liquid phase with a reduced electrical consumption, can lead to substantial advantages in thermodynamic efficiency with respect to pure CO_2 cycles [29]. Therefore the amount of the dopant influences not only the performance of the power block [29] but the thermodynamic properties [30] too. Table 2 reports the main assumptions related to the thermodynamic analysis of the power cycles: while the turbomachinery efficiencies refer to small-scale applications, the maximum pressure (250 bar) is kept at levels of large-scale plants, to not penalize the cycle performance [21,22]. CO_2 mixtures for power cycles at high temperatures are extensively studied in literature within the H2020 EU projects SCARABEUS and DESOLINATION, focusing on concentrated solar power applications.

The selection of a suitable dopant for CO_2 is a matter of thermophysical properties, thermal stability, chemical compatibility, hazards, and cost. Among other dopants selected for CO_2 mixture applications [10,11] and fluorocarbons studied in the literature [31,32], Hexafluoro benzene (C_6F_6) is proposed in this work as dopant, since various works already highlighted its potential in power generation application

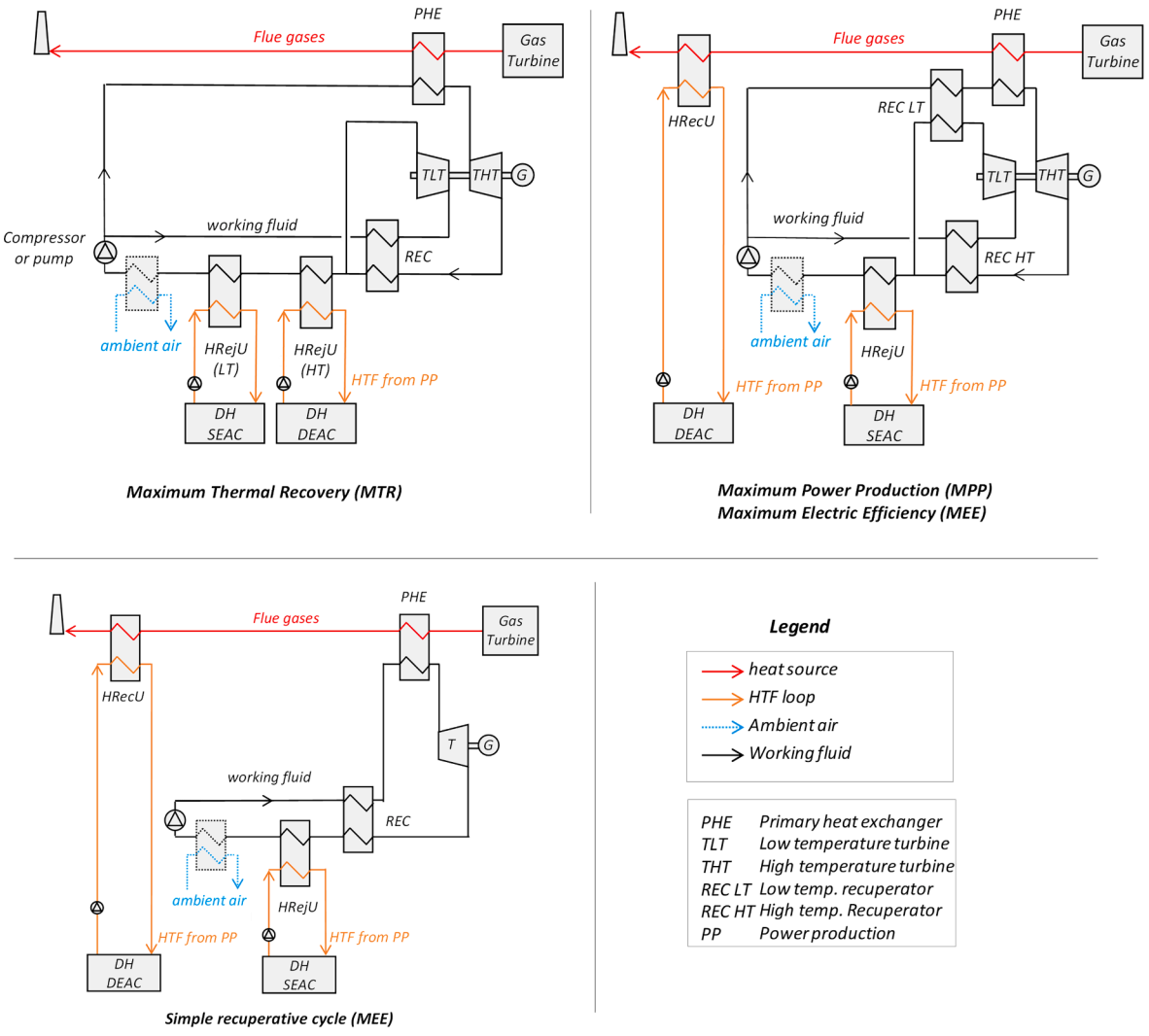

Fig. 3. Cascade cycle: MTR configuration (left – upper), MPP/MEE (right – upper). Simple recuperative MEE (bottom).

Table 2
Power block assumptions.

Cycle Parameter	Value
Cycle maximum pressure	250 bar
Cycle minimum pressure	At bubble point (mixture) Optimized (pure)
Cycle maximum temperature	Optimized
Cycle minimum temperature	50 to 70 °C
PHE minimum temperature approach	30 °C
Recuperators pinch point	10 °C
Pressure drops (PHE/ HRejU)	3 / 1 bar
Recuperator pressure drops (HP/LP)	1 / 2 bar
Isentropic efficiency (turbine/compressor)	85 / 80 %
Generator/Motor efficiency, η_m	97 / 97 %

[23,33–35]. Additionally, it proved high thermal stability (up to 600 °C) [36] and it is already studied in the first-of-a-kind experimental apparatus at TU-Wien [37]. The two working fluids are modelled considering the state of the art of the thermodynamic model already available in the literature. Reduced Helmholtz energy Span-Wagner equation of state [38] has been adopted to model pure CO_2 as it is the reference multi-parameter equation of state for this fluid and the one providing the highest accuracy with respect to experimental data especially close to the critical point where the compressor operates [39]. Differently, the adoption of this complex equation for the mixture results in a poor accuracy with respect to the available experimental data for the mixture. For this reason, the mixture cases have been modelled adopting Peng-Robinson equation of state [36] with an optimization of the mixture binary interaction parameter in accordance with other research works too [34,40,41]. Appendix A lists the properties of the chosen working fluids and the functional form of the mixture binary interaction parameter.

The performance of the CS and SR cycles are quantified by the electrical efficiency η_{EE} (Equation (1), defined as follow:

$$\eta_{EE} = \frac{\sum \dot{W}_t \cdot \eta_m - \dot{W}_c / \eta_m}{\dot{Q}_{PHE}} \quad (1)$$

where $\sum \dot{W}_t$ is the mechanical power produced by both the high (both SR and cascade) and low temperature turbines (cascade only), while $\dot{W}_c$ is the mechanical power consumed by the pump (for CO_2 mixture cycles) or compressor (pure CO_2 cycles).

2.3. Absorption chiller modelling

An absorption chiller produces cold thermal power, typically in the form of chilled water, from a low-medium temperature heat source, exploiting a thermodynamic cycle with a mixture of a refrigerant and an absorbent [42]. The transport of a vapor into an absorbent mixture in either a liquid or solid form is referred to as absorption [43]. Several AC

configurations are commercially available, with different number of pressure levels and various temperature levels of the heat source: in this work both single effect AC (SEAC) and double effect AC (DEAC) are investigated, adopting the H_2O-LiBr (lithium bromide as absorbent) solution [43]. The main characteristics and properties of the two chemical species are recollected in the Appendix A Table 2.

In a SEAC (Fig. 4 – left), the pumped mixture starts with a typical LiBr mass concentration of 50 % to 55 %. After pumping, it's pre-heated in a recuperator (*Rec*) and further heated in the generator (*Gen HP*) until partial evaporation occurs, depending on temperature and pressure. The resulting vapor is condensed using ambient air (*Cond*) and then expanded to evaporation pressure. Pressure levels are determined by saturation conditions of the H_2O-LiBr mixture at temperatures T_{cond} and T_{eva}. In the evaporator (*Eva*), cold thermal power is produced by cooling chilled water. The LiBr-rich flow leaving the generator (strong solution) is then circulated back to the recuperator, expanded through a throttling valve, and fed to the absorber (*Abs*). Here, it's diluted with refrigerant from the evaporator, cooled, and returned to the pump for recirculation.

The plant layout of a DEAC presents an additional pressure level comparing to SEAC and can adopt two different configurations. The series flow layout comprises two generators in series (*Gen HP* and *Gen LP*) and a single pump, while, in the parallel flow layout, the generators are in parallel, and two pumps are necessary [43]. The DEAC solution selected in this study (Fig. 4 – right) is the layout with the generators in series, as it leads to higher COPs than the parallel one [43]. In Fig. 4, the strong solution at the high-pressure generator outlet is expanded to an intermediate pressure, corresponding to the water condensation pressure in the condenser (*Cond*). After that, both the evaporated water and the strong solution flow into the components previously mentioned. The advantage of the double effect layout is to separate more water from the solution, thus increasing the cooling capacity and the cycle performance. Typically, SEAC work at low pressures (down to 7 kPa) meanwhile, DEAC and multi-effect AC work at higher pressure levels (up to 100 kPa), with a heat source temperature up to 160 °C–180 °C, generally resulting in COP above 1 [42]. The presented values of COP are defined Equation (2) as the ratio between the cooling capacity at the evaporator $\dot{Q}_{CC}$ and the thermal input power from the heat source $\dot{Q}_{hs}$ neglecting the electric consumption of the circulation pump [44].

$$COP = \frac{\dot{Q}_{CC}}{\dot{Q}_{hs}} \tag{2}$$

The H_2O-LiBr solution is modelled with the ELECNRTL pre-defined package in ASPEN Plus, as suggested in literature [42]. The boundary conditions and the main assumptions for the simulation of the AC behaviour are aligned with other modelling literature [42,45] (Table 3). The thermal power is provided to the ACs through pressurized water (modelled with a constant specific heat capacity) that works as heat source. The methodology adopted in this work aims at defining the AC performance map displaying the COP as function of heat source maximum temperature T_{hs} and the exploitable temperature difference of the heat source ΔT_{hs} (Table 3). Whilst the maximum pressure of the SEAC is univocally computed and it is thus fixed, corresponding to the water condensation pressure (Table 3), an optimization analysis is carried out for the DEAC configuration to find the operating pressure condition which maximizes the COP value on a case-specific basis. In each condition considered, as reported in Table 3, the problem related to crystallization phenomena, such as piping and components clogging, must be addressed: according to the Dühring chart, the mass concentration of LiBr should be always below 65 % [46].

2.4. Avoided emissions and primary energy saving

CHP and CCHP systems are known for their environmental benefits, including avoided carbon emissions and primary energy savings. In this study, avoided carbon emissions are calculated by comparing emissions from electricity, hot water, and chilled water production in the proposed retrofitted configuration (represented in Fig. 2 right) with those from the existing trigeneration plant. For electricity, emissions are based on the average European emissions from the electric sector of $kgCO_{2,eq}$/MWh in 2021 [47]. Hot water production emissions, including typical efficiencies and losses, are calculated for a district heating system powered

Table 3
Simulation boundary conditions and assumptions for the absorption chiller (both SEAC and DEAC).

Chiller Parameter	Value
Condensation conditions, T_{cond}/P_{cond}	40 °C / 7.38 kPa
Evaporation conditions, T_{eva}/P_{eva}	3 °C / 0.75 kPa
Pump inlet LiBr concentration (mass based)	55 %
LiBr maximum acceptable concentration in strong solution (mass based)	65 %
Minimum approach temperature difference in the generators	5 °C
Pinch point temperature difference in the generators	5 °C
Approach temperature difference in the evaporator	3 °C
Heat source maximum temperature	80 to 160 °C
Heat source temperature difference	10 to 50 °C

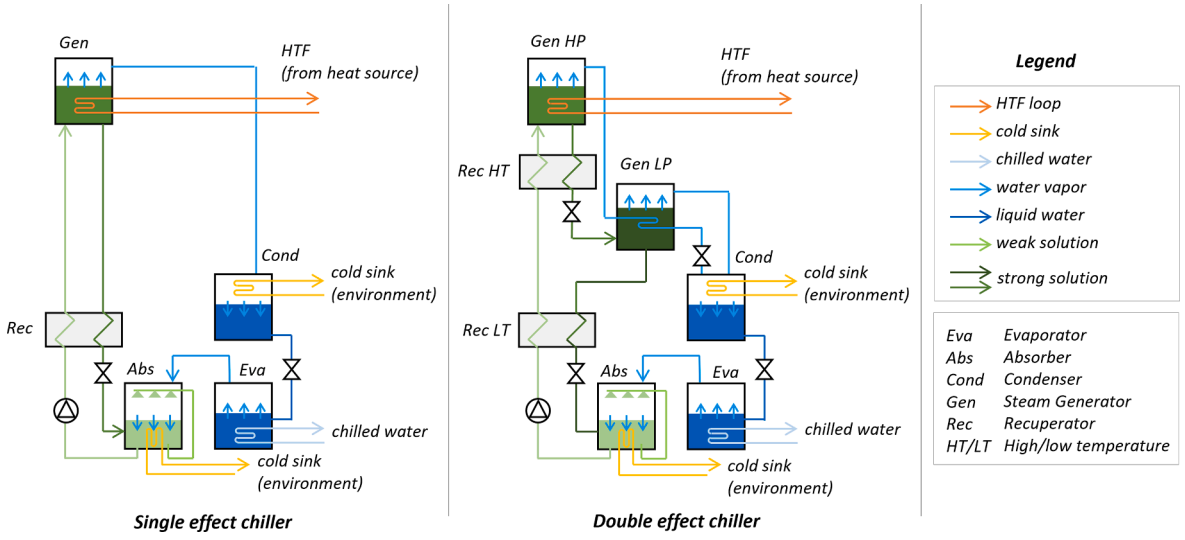

Fig. 4. Absorption chiller layout: single effect (left) and double effect (right).

by natural gas [48], while emissions from compressor chillers are based on the European grid electricity mix. Emission correlating whit the use of the two different fluids are not take into account mainly because adopting a closed cycle the working fluid is not expected to be released in the environment but also because C_6F_6 has a low global warning potential (100 years) of 9 and an ozone depletion potential equal to zero [49] being thus a low environmental impact fluid with respect to other halogenated hydrocarbons. Table 4 provides necessary data for the analysis, including the utilization factor. Operating hours for district heating are from mid-October to early April, while district cooling runs for three summer months. Therefore, the power cycle's operating hours are the sum of these periods, as operating a gas turbine with limited efficiency is not preferable when waste heat cannot be utilized for heating or cooling.

Additionally, the overall efficiency η_{CCHP} is computed based on the annual fuel energy consumption E_{CCHP}, the produced electric E_{EE}, district heating E_{DH} and cooling E_{DC} energy as presented in Equation (3). Eventually, a relevant key performance parameter in a CCHP is the primary energy saving (PES) index, that compares the primary energy consumption of the trigeneration plant with the primary energy that would be consumed in the case of separate production of i) electricity, ii) heat and iii) cold (Equation (4)).

$$\eta_{CCHP} = \frac{E_{EE} + E_{DH} + E_{DC}}{E_{CCHP}} \tag{3}$$

$$PES = 1 - \frac{E_{CCHP}}{\frac{E_{DC}}{\eta_{gb,ref} \bullet COP_{ref}} + \frac{E_{EE}}{\eta_{grid} \bullet \eta_{EE,ref}} + \frac{E_{DH}}{\eta_{gb,ref}}} \tag{4}$$

For the PES calculation, the electric power also includes the production from the gas turbines because it considers the actual primary energy source engine, and its exclusion would always result in 211 GWh_{th}/year on LHV basis from combustion of natural gas in the gas turbines. The term E_{EE} is the sum of the produced electricity with the bottoming CO_2 power cycle and the 10 MW_{el} from the gas turbines. The references efficiencies in the PES formulations for the separate production systems are: i)$\eta_{EE,ref}$, a reference generation efficiency for electricity set at 53 %, ii) $\eta_{gb,ref}$, a reference efficiency for a thermal loads from natural gas boilers, equal to 92 % [50], iii) the COP_{ref} for the production of chilled water, set at 1.1 as average value for DEAC and iv) η_{grid}, a factor equal to 0.952 that accounts for transmission losses in the electricity grid [50].

2.5. Economic analysis adopting high efficiency certification

The economic analysis employs the following methodology: for each case study (combination of working fluid, plant configuration, and cycle design criteria), the electricity cost (LCOE) is computed to achieve a net present value of zero for the overall investment, assuming a reference discount rate. The main assumptions for the economic analysis are outlined in Table 5. This comprehensive analysis considers not only capital and operational expenses (CAPEX and OPEX), but also plant amortization, taxes, and revenues from the sale of electricity, hot and chilled water, including additional income from Energy Efficiency Certificates (EEC).

For the specific cases discussed in this study, the Italian CAR (*Cogenerazione Alto Rendimento* – i.e.: High efficiency cogeneration) regulation for cogeneration and trigeneration power plants is applied [51]. High-performance cogeneration and trigeneration units are rewarded with Energy Efficiency Certificates (EECs) in compliance with European Directive 2012/27 [50]. To qualify for EECs, two conditions must be met: i) the PES index, as defined in Equation (4), must be equal to or higher than 10 %, and ii) the η_{CCHP}, as defined in Equation (3), must exceed a threshold value of 80 % [51]. If the plant falls short of the overall efficiency threshold, the CAR regulation is applied to a specific subsection to ensure alignment with the threshold, following the virtual machine concept. This allows the plant to still benefit from EECs, but only in proportion to the PES of the virtual machine [51], while the remaining part of the plant does not receive incentives. The benefit of high efficiency results in remuneration, lasting 15 years for district heating plants, directly proportional to the primary energy savings evaluated in tonnes of oil equivalent.

The economic analysis methodology is detailed in Appendix B, applying a balanced plant assumption of 20 % of all CAPEX. A discount rate of 8 % and a lifetime of 25 years are utilized. Economic assumptions for CAPEX align with literature values for gas turbines, CO_2 power block, SEAC, DEAC, HRejU, and HRecU. Gas turbine costs are sourced from a gas turbine handbook [52], while CO_2 power plant component costs are computed using Weiland's correlations [53,54]. OPEX refers solely to natural gas consumption, assumed at \$30/kW_{el}y for CO2-based cycles [55]. SEAC and DEAC costs follow assessments by the US Department of Energy [56]. HRejUs and HRecUs are modelled as conventional heat exchangers, with costs sourced from literature [57,58]. Chiller cost correlations are also taken from literature [59], assuming a COP_{ref} of 3 for PES calculations. Equipment costs are actualized using the Chemical Engineering Plant Cost Index [60]. In this analysis, the cost of natural gas as well as the selling price of hot and chilled water and the EEC rate are an average value from 2023. The price of natural gas is 42 \$/MWh_{LHV} (raw material only), while the price of hot water is 120 \$/MWh [52] and 65 \$/MWh [53] for chilled one, and the EEC are evaluated at 250 \$/toe [54].

Four cases, reported in Table 6, have been included in the current economic analysis to compare the current proposed CCHP system against different solutions. *Case 1* refers to a CHP plant composed by the two gas turbines and the HRSG to run the DH, while *Case 2* represents the existing CCHP plant with the compression chillers. *Case 3* corresponds to the scenario where the compression chillers are substituted

Table 4
Data for the avoided emission analysis.

Production	Yearly utilization factor [%]	Operating hours [h/year]	Specific emission [$kgCO_{2,eq}$/MWh]
Electricity	70	6120	234
Hot water	45	3960	274
Chilled water	25	2160	78

Table 5
Main assumption for the economic analysis.

Parameter	Value
CCHP Lifetime	25 years
Amortisation time	10 years
ECC time	15 years
Discount rate	8 %
Tax rate	43 %
Cost of balance of plant	20 % of the total CAPEX
Cost of natural gas	42 \$/MWh_{LHV}
Selling price of hot water	120 \$/MWh
Selling price of chilled water	65 \$/MWh
Revenues from EEC	250 \$/toe (21.5 \$/MWh)

Table 6
Summary of the additional cases analysis.

Case	Description
Cases CO_2	Two gas turbines, CO_2 bottoming cycle, SEAC, DEAC, HRejU and HRecU
Case 1	Two gas turbines and HRSG for hot water
Case 2	Two gas turbines, HRSG for hot water and compression chillers for chilled water
Case 3	Two gas turbines, HRSG for hot water and DEACs for chilled water
Case 4	Two gas turbines, HRSG for hot water, compression chillers and DEACs for chilled water

with DEACs that fully exploit the thermal energy from the flue gases. Finally, *Case 4* considers the existing CCHP with the addition of DEACs as in *Case 3*.

3. Results and discussion

This chapter reports and discusses the results of this work. Starting from the thermodynamic analysis of the system, which is location-independent and in principle can be representative of other applications, it is also discussed how the power blocks and the DH/DC are coupled. A last section is focused on the economic and environmental performance of the system, evaluated for the case study of the trigenerative plant located in northern Italy.

3.1. Performance maps of the absorption chillers

The resulting trends of the COP for both absorption chillers configurations are reported in Fig. 5, referring to the plant layouts of Fig. 4 and the assumptions on the cycle characteristics of Table 3. For SEAC, the T_{hs} is varied from 80 °C to 120 °C, while for DEAC from 120 °C to 160 °C and for both configurations the ΔT_{hs} ranges from 10 °C to 50 °C.

For both categories of AC, higher COP are computed at high T_{hs} and low ΔT_{hs} (close to an isothermal hot source), with a plateau reached at a value of T_{hs} equal to 100 °C and 150 °C for the SEAC and DEAC, respectively. In the SEAC the pressure level is fixed by the condensation condition, and an increment of the T_{hs} corresponds to a higher water vapor fraction, leading to a higher cooling capacity while decreasing the ΔT_{hs} implies a higher internal regeneration of the AC. Therefore, at high T_{hs} the COP is favoured by a greater steam production while low ΔT_{hs} limited the $\dot{Q}_{hs}$ introduction. In the DEAC simulations, on the other hand, the COP is maximized for each condition by varying the maximum pressure which is a free design variable in this case. Therefore, for this configuration the previously mentioned effects are evident, and it becomes possible to achieve a COP in the range between 1.25 and 1.45 even with relatively low T_{hs} (130-160 °C) and large ΔT_{hs} (30-50 °C). A significant drop in COP can be noted when T_{hs} is equal to 120 °C and the temperature difference is greater than 20 °C, reaching values comparable to SEAC for the same heat source characteristics.

Considering the DEAC configuration, the optimum values of the high-pressure level of the cycle vary from 50 kPa to 105 kPa and maximum pressure increase mainly depends on the heat source maximum temperature T_{hs}: for each case, the limit is set by constraints related to the crystallization of the mixture. Differently, in a SEAC, the vapor generation and thus the LiBr concentration in the strong solution, are directly proportional to the increase of T_{hs}, thus the maximum pressure is set by T_{cond} and, as depicted in Fig. 5, this value is equal to 40 °C up to a T_{hs} lower than 100 °C while for higher heat source temperature the T_{cond} and consequently P_{cond} must increase to keep the strong solution LiBr concentration below 65 %. Nevertheless, an increase of T_{hs} over 100 °C in SEAC leads to a penalization of the COP since the rising of the temperature is counterbalanced by the increase of P_{cond}. The optimum COP has been fitted in a polynomial regression obtained by OLS method in the functional form of Equation (5) with an R^2 equal between 0.983 and 0.999. Coefficients to be adopted in the correlations are reported in Appendix A while the code used for the post processing for the Aspen results is reported in the Supplementary Material.

$$COP(T_{hs}, \Delta T_{hs}) = a_{00} + a_{10}T_{hs} + a_{01}\Delta T_{hs} + a_{02}T_{hs}^2 + a_{11}T_{hs}\Delta T_{hs} + a_{02}\Delta T_{hs}^2 + a_{30}T_{hs}^3 + a_{21}T_{hs}^2\Delta T_{hs} + a_{12}T_{hs}\Delta T_{hs}^2 + a_{03}\Delta T_{hs}^3 \quad (5)$$

In conclusion, in order to match efficiently the AC with the considered temperature range of the thermal source available, the optimal T_{hs} is found at 95 °C for the SEAC and at 150 °C for the DEAC (values that correspond to the maximum achievable COP), while the ΔT_{hs} should be chosen in accordance to the considerations presented in the following chapters, on a case-specific basis. It is worth noticing that the AC performance maps provided in this chapter can be considered valid independently from the application investigated in this work, and thus are valuable results for any future literature works that focuses on the investigation of the performance of absorption chillers with a conventional H_2O-LiBr mixture as working fluid.

3.2. Performance of the CO_2-based power cycles

This chapter presents the cycle efficiency results of both CO_2 and transcritical CO_2-mixtures power cycles analysed in the trigeneration plant case study. In the cascade cycle, optimal cycle minimum pressure remains relatively constant for CO_2 cycles in MTR and MPP configurations. Differently, reducing cycle maximum temperature has opposing effects: it increases heat input by lowering recuperator outlet temperature but decreases cycle efficiency due to reduced enthalpy drop at the expander. Despite this, the net power output varies by less than 1.5 % in the optimal range of 440 °C to 480 °C for maximum cycle temperature, while for MEE, the highest cycle efficiency occurs at a turbine inlet temperature of 480 °C (compatible with the minimum approach

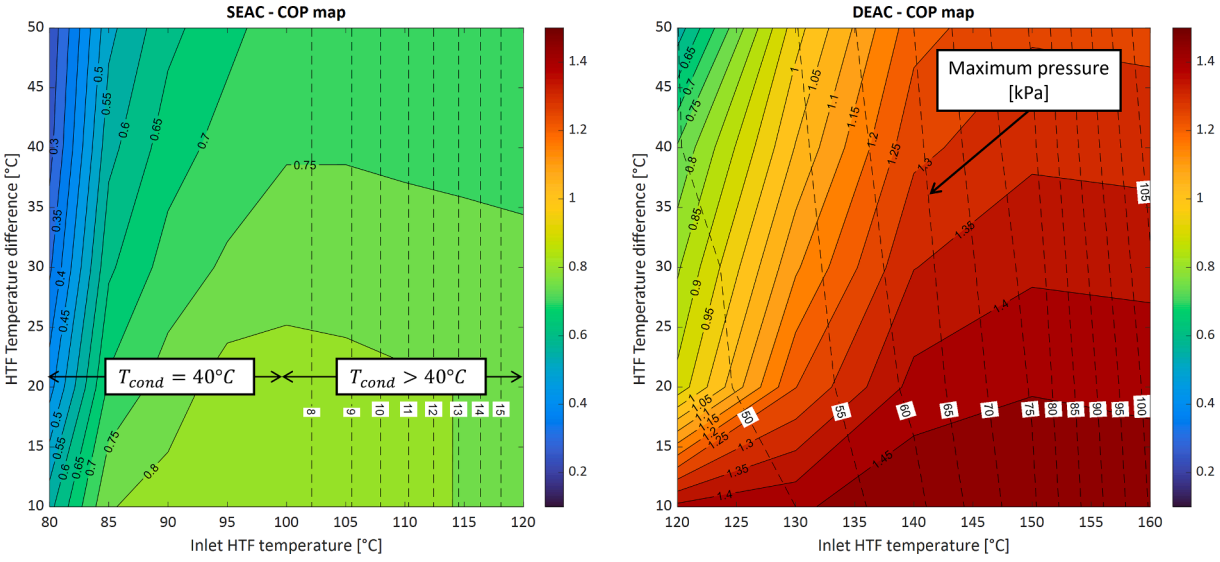

Fig. 5. COP maps for single effect AC (left) and double effect AC (right).

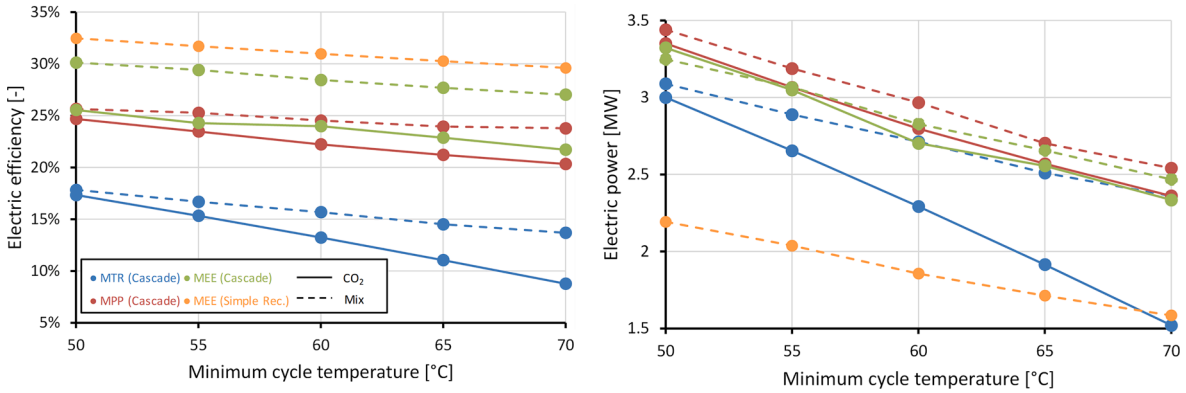

Fig. 6. Electric efficiency (left) and electric generation (right) as function of the minimum cycle temperature.

temperature difference in PHE). Fig. 6 illustrates the trend of electric efficiency and power output for all cycle combinations, varying cycle minimum temperature. The results presented here refer only to optimal cases and nominal conditions.

Increasing T_{min} normally implies a penalization of the cycle performance due to the increment of the specific volume of the compressed flow (for pure CO_2 cycles) and the reduction of the pressure ratio (for blended CO_2): nevertheless, this penalization effect is more marked for the pure CO_2 cases since transcritical cycles always benefit from a compression process in liquid phase where variation of pressure and temperature only lead to marginal changes in the working fluid volumetric behaviour.

Among the different cascade cycle configurations, the MTR cycle with CO_2 is the most penalized one since the need of ensuring a complete heat source cooling in the PHE leads to a limitation of the cycle pressure ratio that eventually involves cycle minimum pressures higher than the optimal ones: all these effects are amplified when the cycle minimum temperature increases. While the use of pure CO_2 always leads to the lowest efficiency and power production, it is interesting to note that the MTR cycle with the CO_2 mixture for high cycle minimum temperature can get a power output close to the other cycles because the lower efficiency is compensated by and higher recovery factor with respect to both MPP and MEE configurations. The CS cycle featuring also the second recuperator in both MPP and MEE cases outperforms the MTR thanks to a more effective regeneration. While for MTR the recovery factor is always maximized, the MPP presents a $0.63 < \chi < 0.74$ (pure CO_2) and $0.58 < \chi < 0.73$ (blended CO_2), which are higher values comparing MEE: $0.59 < \chi < 0.71$ (pure CO_2) and $0.53 < \chi < 0.62$ (CO_2 mixture). Concerning the mixture, the analysis underlines that the optimal molar fraction of C_6F_6 varies from 8 % to 13 % in MPP and MTR configuration, and from 17 % to 20 % in the MEE configuration. This results are consistent with the work of Di Marcoberardino [36], where the maximum efficiency is reached at C_6F_6 molar fraction of 18 % and the maximum specific power at 10 %. In the MEE case, the turbine inlet temperature (TIT) is set to the maximum value of 480 °C, compatible with the constraint on the minimum pinch temperature at the PHE since an increase of this parameter is always beneficial for the electric efficiency. At the same TIT, the use of mixture allows for a higher thermodynamic efficiency (around + 3 % with respect to CO_2), thanks to more balanced heat capacities within the recuperators. Nevertheless, adoption of pure CO_2 allows to lower the PHE inlet temperature because of a more unbalanced recuperator, leading to higher heat recovery ratios and thus leading to higher electrical output. While this effect is evident at low cycle minimum temperature, at high temperatures the efficiency of the CO_2 cycles remarkably drops compared to the use of mixture due to the increase of the compressibility factor. Regarding the MPP design, which represents the trade-off between the heat source cooling grade and the cycle efficiency, the use of mixture outperforms the adoption of pure CO_2 even if the optimal TIT is around 10 °C lower, providing a more effective heat source cooling, without involving a substantial cycle efficiency penalization. In fact, pure CO_2 suffers both from the distance from the critical point in the compression step and from the unbalanced heat capacity in the recuperators, while the mixture can adapt the composition to exploit the benefits of liquid compression and balanced heat capacities at recuperator.

Those considerations on the cascade layout are also valid for the simple regenerative one. High efficiency is reached when TIT is equal to 480 °C and the C_6F_6 molar fraction ranges from 15 % to 19 %. The electric efficiency η_{EE} is computed from 32.4 % to 29.6 %, significantly higher than blended CO_2 MEE with cascade layout. The power production of the SR cycles is computed between 1.6 and 2.2 MW_{el} lower than blended CO_2 MPP and comparable with MTR at high minimum temperature cycle. In fact, in the simple recuperative cycle, the regeneration inside the cycle permits the working fluid to enter at higher temperature inside the PHE, with a limited exploitation of the heat source. Nevertheless, the most noteworthy outcome is the low recovery factor which varies from 0.28 and 0.35, meaning that the quality of the heat after the PHE is relevant.

3.3. Heat recovery optimization in winter and summer operation

Thermal power is transferred to the intermediate loop through the HRecU, which cools down flue gases to stack temperature, and the HRejU, which collects heat released by the cycle. After defining cycle thermodynamic conditions based on the three design criteria in section 3.2, heat integration with adsorption chiller units and district heating is optimized for summer and winter operation. Optimal heat recovery is mainly related to the available maximum temperatures in HRejU and HRecU units (Table 7). These temperatures increase with higher T_{min} and adopting transcritical mixture, compared to pure CO_2, due to energy balance across the recuperator and PHE.

For the first component (REC in MTR configurations and REC HT in

Table 7
Available maximum temperature of the working fluid in the HRejU and the flue gases in the HRecU. HRecU is not presented in MTR configuration. Temperature in [°C].

T_{min}	Heat Source	CO_2 MTR	CO_2 + C_6F_6 MTR	CO_2 MPP	CO_2 + C_6F_6 MPP	CO_2 MEE	CO_2 + C_6F_6 MEE	CO_2 + C_6F_6 SR
50	Working fluid	182	175	104	94	97	96	92
70	Working fluid	214	206	139	113	126	114	112
50	Flue gases	–	–	224	227	236	272	370
70	Flue gases	–	–	266	287	285	308	399

MPP and MEE ones – Fig. 3), the minimum pinch point is located at the cold end of the heat exchanger. As the outlet temperature of the compression depends on the pressure ratio and T_{min}, the hot side outlet temperature of the recuperator, corresponding to the maximum available temperature in HRejU, is uniquely determined. Due to the impact of the energy balance at the PHE, the high electric efficiencies in MEE layouts result in incomplete exploitation of the thermal source, leading to higher temperatures compared to MTR and MPP configurations.

3.3.1. Winter season heat management

During the winter season, the district heating generation operates with fixed return and supply temperatures (60 °C and 95 °C, respectively), limiting the degree of freedom in the system design and operation.

In MTR cycles, heat is solely collected from the HRejU (cooling/condensation of the working fluid) as the flue gases are fully cooled down within the cycle. The available heat for district heating is calculated based on the HTF inlet and outlet temperatures (65 °C-100 °C), and the assumed pinch point temperature difference (5 °C). Any thermal power released by the cycle below 70 °C is rejected with an air-cooled unit (Fig. 7). In contrast, MEE and MPP configurations allow heat collection from both the HRejU and the HRecU (final cooling of the flue gases). The HTF minimum temperature remains fixed (65 °C), but the outlet temperature from the HRecU heat exchanger must be optimized to maximize overall collected thermal power while keeping constant the final HTF mixing outlet temperature (100 °C). Increasing the HTF outlet temperature from the HRecU can optimize heat recovery while respecting minimum pinch point constraints because it allows to increase the temperature of the HTF from the HRejU before the DH section. In all cases, heat from the flue gases (HRecU) is fully utilized, with an air cooler unit required for the HRejU depending on T_{min}.

3.3.2. Summer season heat management

In summer operation, maximizing cooling capacity involves using a combination of single and double-effect absorption chillers fed by different high-temperature HTF loops. The arrangement of heat exchangers for recovering power for the chillers varies based on the cycle architecture. In MTR cycles, heat is obtained solely from cooling or condensation of the working fluid in the HRejU, utilizing SEAC, DEAC, or a combination of both.

With SEAC, it is convenient to adopt a HTF inlet temperature (T_{hs} in section 3.1) higher than the cycle minimum temperature to maximize the heat recovery, and to increase the HTF difference temperature (ΔT_{hs} in section 3.1) to maximize the COP while respecting both the limits on the maximum HTF temperature for SEAC and on the minimum HRecU pinch point temperature difference. With DEAC, both the minimum and the maximum temperature of the HTF shall be optimized to find the optimal trade-off between the heat recovery efficiency and the DEAC COP.

For pure CO_2 MTR case at $T_{min} = 70^{\circ}C$ the maximum cooling capacity with only SEAC is 12.65 MW_{th} ($T_{hs} = 95^{\circ}C$ and $\Delta T_{hs} = 30^{\circ}C$) while it is equal to 12.2 MW_{th} for the only DEAC ($T_{hs} = 150^{\circ}C$ *and* $\Delta T_{hs} = 35^{\circ}C$). It can be noticed that for the DEAC case it is preferrable to penalize a bit the COP (adopting 140 °C as T_{hs} rather than 150 °C) to increase the heat recovery turning out in a positive effect on the cooling capacity. The third case adopts two HTF loops: one for the SEAC and the other, at higher temperature, for the DEAC, placed in series in a counterflow heat exchanger with the condensing fluid. For this case, by optimizing the HTF loops temperature ($T_{hs} = 150^{\circ}C$, $\Delta T_{hs} = 35^{\circ}C$ for DEAC and $T_{hs} = 95^{\circ}C, \Delta T_{hs} = 30^{\circ}C$ for SEAC) the heat is completely exploited, 53 % for the high temperature loop and 47 % for the low temperature one (Fig. 8). The overall cooling capacity is 18.32 MW_{th} for the case study of this work, equal to + 44 % with respect to the SEAC only and + 50 % with respect to the DEAC only, thus making this more complex heat recovery arrangement for MTR cycles likely preferrable also from techno-economic perspective.

For MEE and MPP, heat recovery from the HRejU is suitable only for powering a SEAC, as the initial condensation temperature is too low for a DEAC. However, heat from the flue gases in the HRecU can be utilized in various ways, leading to different HTF loop architectures.

In most complex configuration, three absorption chillers are employed: one DEAC receives heat from the high-temperature flue gases, while two SEACs receive heat from the HRejU and the final flue gas cooling, respectively. These HTF loops in the HRecU are arranged in series and counterflow with the flue gases, offering maximum flexibility and allowing for optimal cooling capacity.

Second case adopts a two-stage cooling process of the flue gases where the two low temperature HTF loops (the one integrated in the HRejU and the one in the low temperature part of the HRecU) are connected to the same SEAC, thus having the same HTF inlet temperature while the outlet HTF temperatures from the two units must be optimized considering the constraint on the HRejU pinch point temperature difference and the effect on SEAC COP. The optimization of the first layout, valid for all the cases, is here presented for the blended CO_2 MEE case at $T_{min} = 70^{\circ}C$ and the pure CO_2 MPP case at $T_{min} = 50^{\circ}C$ case, that are respectively the cases having the largest and the lower values of both the flue gas inlet temperature (308 °C and 224 °C) and the available thermal power (8.7 MW and 4.8 MW) in the HRecU.

In case of blended CO_2 cycle in MEE configuration at $T_{min} = 70^{\circ}C$,

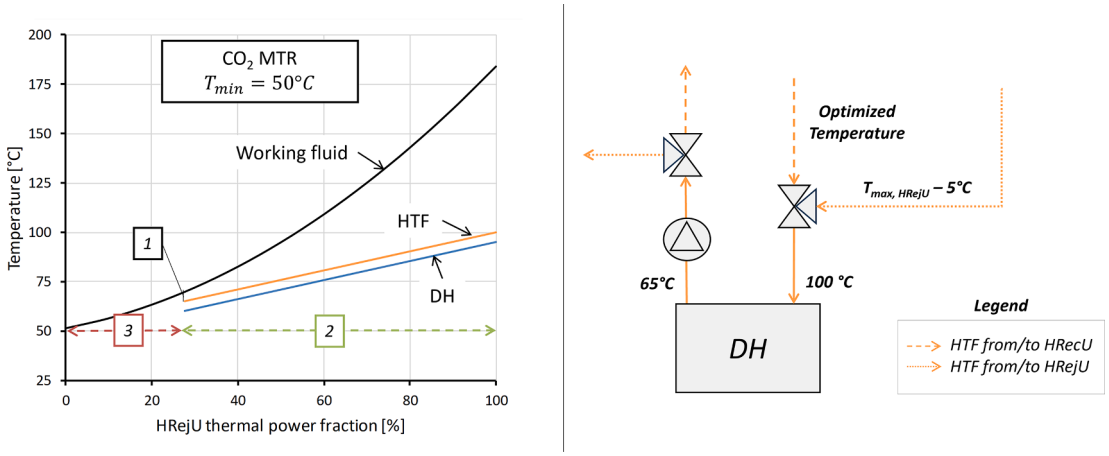

Fig. 7. Left: Examples of coupling of the HRejU with the temperature range of the intermediate HTF loop and the district heating network: pure CO_2 MTR at $T_{min} = 50^{\circ}C$. Legend: [1] Temperature approach, [2] useful fraction of the thermal power and [3] dissipated fraction of the thermal power by the air cooler. Right: Adopted strategy for DH scope in MPP and MEE mode.

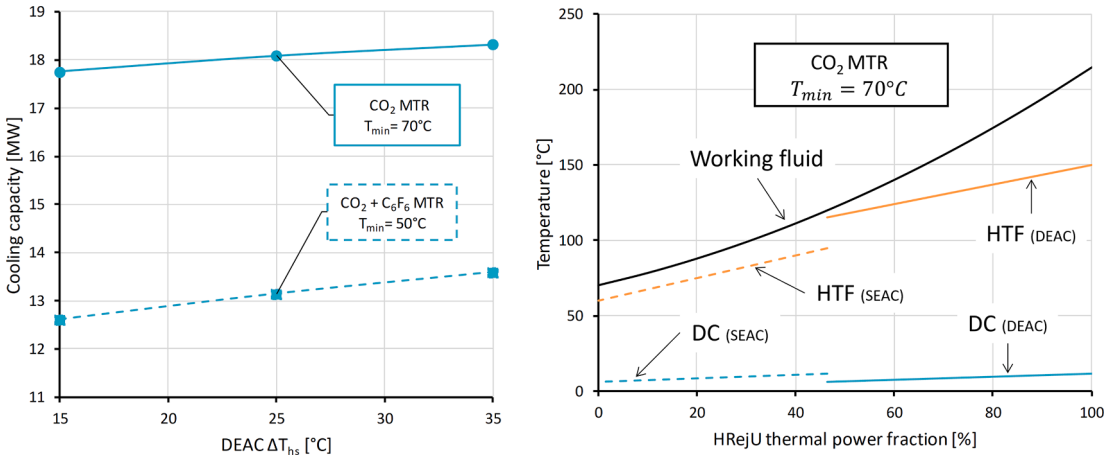

Fig. 8. Examples of coupling of the HRejU with the temperature range of the intermediate HTF loop and the district cooling network for MTR configuration. Left: MTR mixture at $T_{min} = 50^{\circ}C$ and MTR pure CO_2 at $T_{min} = 70^{\circ}C$ cooling capacity vs DEAC ΔT_{hs}. Right: Optimum matching for MTR pure CO_2 at $T_{min} = 70^{\circ}C$.

the optimal HTF loops temperatures in the HRecU unit are respectively $T_{hs} = 95^{\circ}C$ and $\Delta T_{hs} = 15^{\circ}C$ for the low temperature loop to maximize heat recovery from flue gases and $T_{hs} = 150^{\circ}C$ and $\Delta T_{hs} = 15^{\circ}C$ for the high temperature loop to optimize the DEAC COP. Around 89 % of the overall thermal power is collected in the high temperature HTF, while the remaining 11 % in the low temperature HTF, allowing to produce a maximum cooling capacity of 12.15 MW_{th} (10.4 MW_{th} from DEAC and 0.75 MW_{th} from SEAC) (Fig. 9 – right). However, it is important to notice that if the heat available from flue gases is used only for a high temperature HTF loop, the optimal T_{hs} and ΔT_{hs} would be 150 °C and 35 °C, maximizing the heat recovery at the expenses of a lower COP, leading to a cooling capacity from the flue gases heat recovery of 11.81 MW_{th}, thus only 0.34 MW_{th} lower (−2.7 %) (Fig. 9 – left) with respect to the most integrated case.

Differently, for the pure CO_2 MPP case at $T_{min} = 50^{\circ}C$ the optimization of the most integrated condition leads to the removal of the low temperature HTF loop in the HRecU, thus releasing heat only to the high temperature HTF loop connected to the DEAC.

Based on the results of those two extreme heat recovery conditions, the only architecture considered in the economic assessment of MTE and MPP cycles is the simplest one: in this configuration, a low temperature HTF loop is fed by the HRejU and connected to a SEAC, while a high temperature HTF loop receives heat from the HRecU and is connected to a DEAC. For both loops the HTF minimum and maximum temperatures are optimized in order to maximize the cooling capacity while respecting the constraints on minimum pinch point temperature differences. Table 8 ultimately summarizes the adopted and suggested strategy for the scope of this work.

Table 8
Adopted strategy for matching the DC and the power block.

Cycle configuration	MPP and MEE	MTR
HRecU strategy	Fully exploited	Not available
AC type	DEAC	–
COP	1.36	–
T_{hs}	150 °C	–
ΔT_{hs}	35 °C	–
HRejU strategy	Full exploitation	Optimized exploitation
AC type	SEAC	SEAC and DEAC
COP	Depending on T_{min}	Depending on T_{min} / 1.36
T_{hs}	95 °C	95 °C / 135 °C
ΔT_{hs}	Depending on T_{min}	Depending on T_{min} / 35 °C

3.4. Energy balance and system efficiency for the case study at nominal conditions

In the CCHP plants studied in this work as case study, the nominal power available is a direct consequence on the adopted strategy proposed in section 3.3. In the summer season, the totality of the remaining heat from the flue gases and the heat available from the working fluid

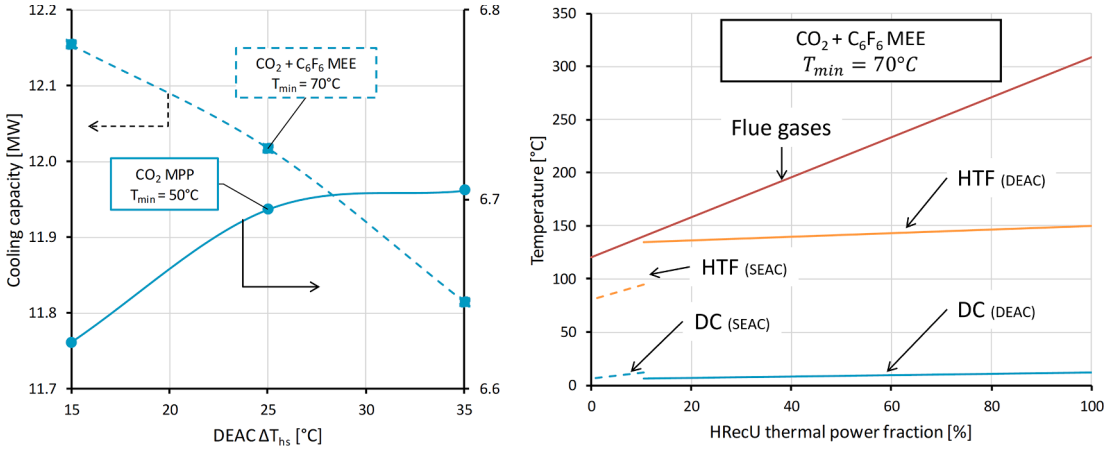

Fig. 9. Examples of coupling of the HRecU with the temperature range of the intermediate HTF loop and the district cooling network. Left: MEE mixture at $T_{min} = 70^{\circ}C$ and MPP pure CO_2 at $T_{min} = 50^{\circ}C$ cooling capacity vs DEAC ΔT_{hs}. Right: Optimum matching for MEE mixture at $T_{min} = 70^{\circ}C$.

cooling (pure CO_2) or condensation (mixture) is recovered, while, due to the rather high value of the DH return temperature, the recovery from the HRejU is not complete in winter operations with the exception of the case with $T_{min} = 70^{\circ}C$. In particular, the power cycle based on the CO_2 mixture running in MEE and MPP mode reject a large amount of low-temperature thermal power to the cooling air, since the maximum temperatures in the HRejU (94 °C and 96 °C as in Table 7) that do not match the DH temperature range (60–95 °C).

Considering the nominal power delivered by the gas turbines of 10 MW_{el} in the current configuration (Table 1), an increment of electric power from 1.5 MW_{el} to 3.4 MW_{el} is possible with the bottom CO_2-based cycles, depending on the configuration, with an available thermal power for DH that ranges from 8.2 MW_{th} to 16.7 MW_{th}, and Thermal power for the absorption chillers connected to the DC network in the range around 16 MW_{th}. It is worth noting that, at $T_{min} = 70^{\circ}C$, the pure CO_2 MTR and the blended CO_2 MEE with a SR layout present almost the same power balance, even if the blended CO_2 MEE cycle has a significantly higher electrical efficiency (29 % vs 8 %), due to the more effective internal recovery process. Even at $T_{min} = 50^{\circ}C$ the SR cycle minimizes the thermal power rejected to the air cooler, as most of it (11.6 MW_{th}) is available at high temperatures.

Fig. 11 summarizes the resulting annual produced energy according to the utilization factors reported in Table 4 and the power balance of Table 1. The original CCHP layout provides 61.2 GWh/y of electricity, 63.4 GWh/y of hot thermal load and 16.2 GWh/y of cold thermal power. Comparing these values to the results shown in Fig. 11, the increase in electric production related to the bottoming power cycles is evident, while, for the same reason, the DH capacity is strongly penalized. However, thanks to the full recovery of the sensible heat in the absorption chiller, the DC capability in the new configuration exceeds the previous one, underlining that the match between absorption chillers and the power cycle HR is an excellent solution for heat recovery.

3.5. Primary energy savings and avoided emissions

In terms of overall efficiency, η_{CCHP} is approximately 82–83 % considering $T_{min} = 70^{\circ}C$ for all the design criteria and both pure and blended CO_2. Decreasing the CO_2-based cycle minimum temperature, $T_{min,cy}$, leads to a lower η_{CCHP}: especially for mixture CO_2 in MPP and MEE configurations the overall efficiency is found at around 68–69 %, due to the great amount of unexploited thermal power in HRejU (see Fig. 10). The SR cycle is the only configuration capable to achieve an overall CCHP efficiency above 80 % at $T_{min} = 50^{\circ}C$. Its good performance are also confirmed by considering the PES index (defined as reported in Equation (4) and shown in Fig. 12), that is proved to be above the threshold limit of 10 % for cycles with $T_{min} = 70^{\circ}C$, with limited differences between the three different design criteria and cycles solutions. At low values of T_{min} the major contribution to the PES is given by the avoided fuel consumption related to electricity generation, while at T_{min} of 70 °C high PES are obtained thanks to the large hot and cold energy production. In the economic results reported in Section 3.6, the mechanism of the virtual machine is applied for the cases with $T_{min} = 50^{\circ}C$, with exception of the blended CO_2 MEE, while all SR and $T_{min} = 70^{\circ}C$ cycles have fully access to the EEC benefits. A sensitivity analysis on the operative hours of the turbine is carried out: increasing the annual capacity factor has clearly a beneficial effect on the electricity generation E_{EE} and the corresponding remuneration, but at the same time it increases the primary energy consumption, E_{CCHP}, without increasing heating and cooling yield thus penalizing the PES index. In fact, assuming 8000 h/y of gas turbine operation, the PES index drops to values between 1 % to 8.5 % and, even with the virtual machine mechanism, the proposed CCHP plant would be economically not profitable.

The CO_2 avoided emissions are calculated on a yearly basis according to the assumptions of Table 4. When T_{min} is equal to 50 °C, the proposed CCHP has a higher equivalent carbon emission than the existing configuration of the trigeneration plant considered (referring to Fig. 13). These higher levels of emission are due to the penalization of the thermal load in winter, that must be compensated by the auxiliary natural gas boilers. The large wasted thermal power in HRejU penalizes mostly the blended CO_2 power cycle, in particular in MPP design where the increase is 2.8 $ktCO_{2,eq}/y$.

The break-even point of the avoided emission is found at T_{min} of around 60 °C, depending on the working fluid and design criteria. In general, all the considered cases are penalized in the retrofitted configuration, with respect to the existing plant, in terms of thermal power to the district heating (during winter), that leads to an additional contribution in emission. Nevertheless at T_{min} of 70 °C the overall avoided emissions are positive (actually avoiding carbon emission with respect to the reference case), ranging from 3.8 (blend CO_2 MPP) to 5 $ktCO_{2,eq}/y$ (SR), due to the positive effect of the high cooling load E_{DC} on the emission balance.

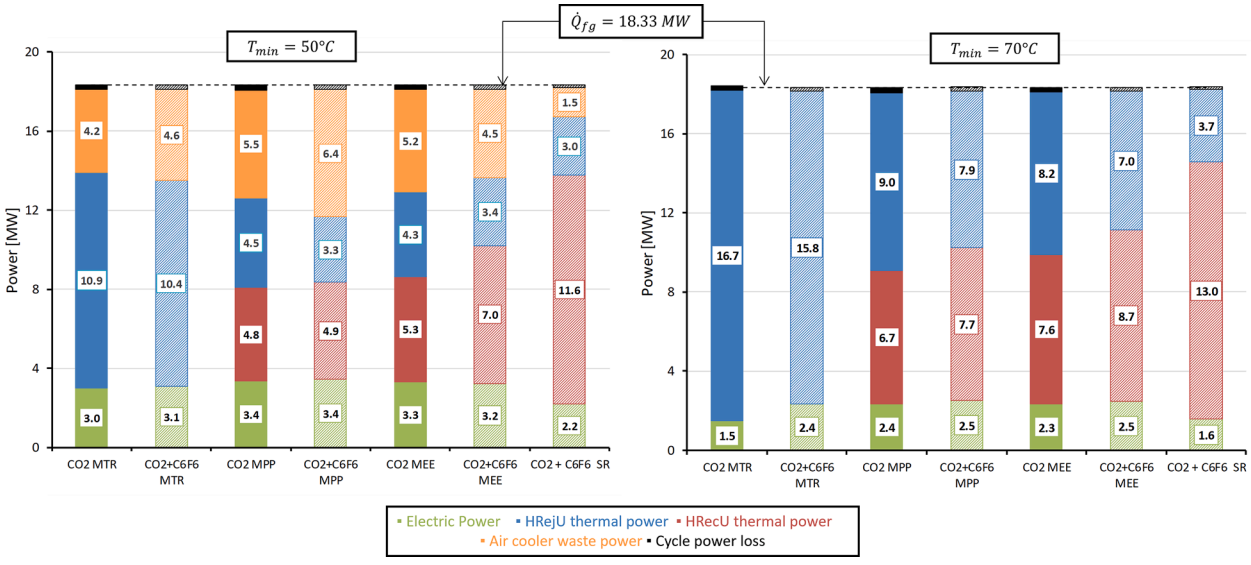

Fig. 10. Power balance for $T_{min,cy} = 50^{\circ}C$ (left) and $T_{min,cy} = 70^{\circ}C$ (right) in winter season.

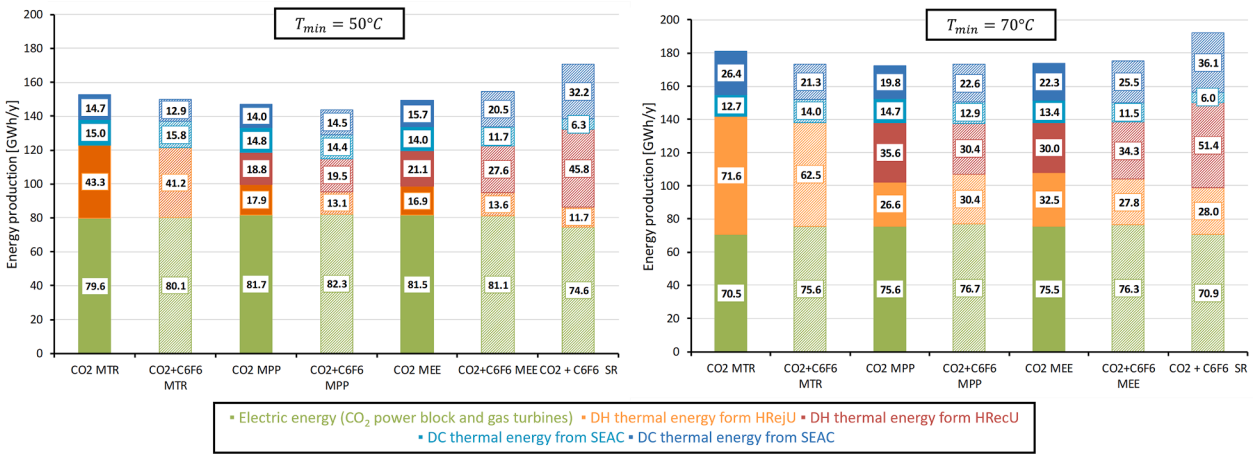

Fig. 11. Annual energy production for $T_{min} = 50^{\circ}C$ (left) and $T_{min} = 70^{\circ}C$ (right).

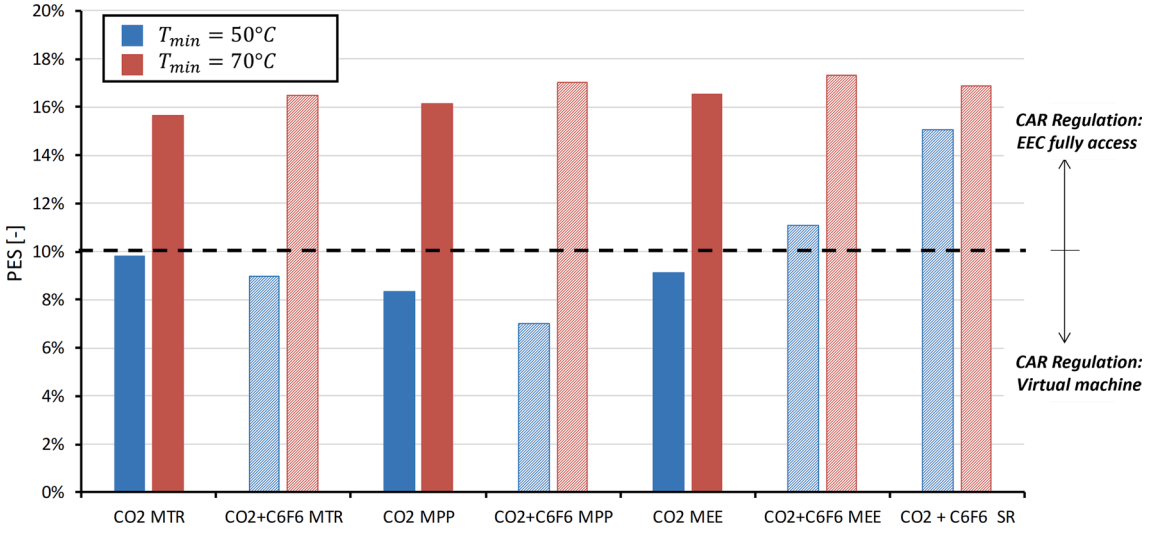

Fig. 12. PES Index for $T_{min} = 50^{\circ}C$ and $T_{min} = 70^{\circ}C$.

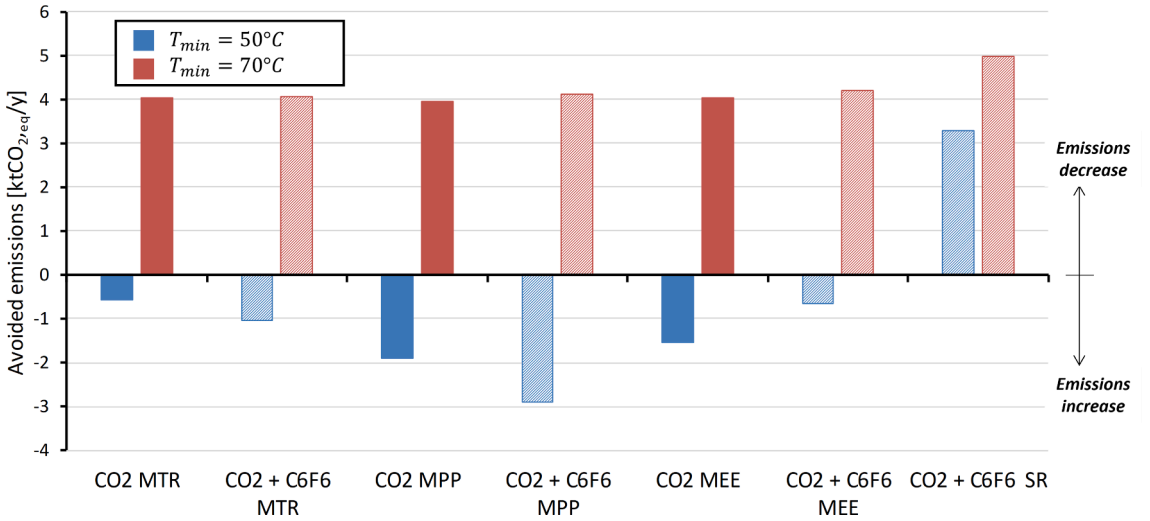

Fig. 13. Avoided emissions for $T_{min} = 50^{\circ}C$ and $T_{min} = 70^{\circ}C$.

3.6. Economic analysis

As mentioned in the methodology, the aim of the economic analysis is to calculate the LCOE that set to zero the net present value of the proposed CCHP plant. Power cycle CAPEX for the components ranges from 7.4 and 9.6 M$ for the cascade cycle (from around 2640 to 4920 $/kW$_{el}$). The MTR configuration presents the lower CAPEX as it adopts only one recuperator, while it exhibits the higher cost of the PHE (from 33 % to 40 % of the total investment) due to the full exploitation of the flue gases thermal power, and the higher specific cost due to the lower rated power. Uncertainty regarding power cycle CAPEX has been introduced considering cost uncertainty for each individual component as proposed by Weiland [53], while uncertainties for absorption chillers and additional HTF heat exchangers has been neglected. The overall combined uncertainty for only the power block CAPEX is ± 34 %. The CAPEX for the SEAC and DEAC are almost the same order of magnitude of the power block investment. The correlations proposed in literature do not take into account the scale factors [56], therefore the cost of SEAC and DEAC are directly related to their cooling capacity. Pure CO_2 MTR and blended CO_2 MEE at $T_{min} = 70^{\circ}C$ (Fig. 14) have the higher absorption chillers CAPEX which is equal to 16.04 M$ and 15.2 M$ (with very similar specific cost between 880 and 890 $/kW$_{th}$), mainly affected by the large cooling capacity of the DEAC. The HRejU and HRecU dimensions (i.e. heat exchange area) are computed according to the plant conditions in summer, representative of the most critical operating condition, as the average temperature difference between the hot and cold flows is lower in summer. The cost of the HRecU gives the major contribution between 350 k$ and 370 k$, while the HRejU stands between 70 k$ and 98 k$ for the cascade layout.

On the contrary, the SR cycle has an power block investment cost ranging from 5.4 to 5.7 M$ (from 1950 to 2560 $/kW$_{el}$) due to the smaller PHE and the use of a single turbine, while the absorption chillers CAPEX is 17.18 M$ (880 $/kW$_{th}$) and the total cost of the HRejU and HRecU is in line with the previous results for $T_{min} = 70^{\circ}C$.

The EEC income is directly proportional to the primary energy saving: more than 3100 certificates are granted for the simple recuperative, blended CO_2 MEE and MPP at $T_{min} = 70^{\circ}C$, while for pure CO_2 MTR the total amount of EEC is 2780, with a revenue per single certificate of 250 $/toe. Thanks to the adoption of the virtual machine mechanism, the case considering $T_{min} = 50^{\circ}C$ can still benefit from the incentives (EEC from 2000 to 2200), however they are not competitive compared to the cycles adopting $T_{min} = 70^{\circ}C$.

As reported in Table 9 and considering the cascade cycles, the pure CO_2 in MTR configuration presents the lower LCOE (31 $/MWh$_{el}$), while there is not an evident difference between MPP or MEE configurations and the use of pure CO2 or mixture. Even though the $T_{min} = 50^{\circ}C$ cycles gain a considerable number of certificates, the LCOE is found at around 66 to 82 $/MWh$_{el}$ because of the low profits in the sale of hot and cold water compared to cases with a higher minimum cycle temperature. In fact, the annual remuneration for cycles with $T_{min} = 50^{\circ}C$ varies from 3.91 M$ for the mixture MPP cycle to 5.19 M$ for the MTR configuration adopting pure CO_2. The revenue from the sale of chilled water ranges from 1.86 M$ (blended MTR) to 2.09 M$ (blended MEE). In contrast, the cycle at $T_{min} = 70^{\circ}C$ presents an average income increase of 2 M$ and 0.5 M$ from hot and chiller water respectively.

Table 9
LCOE in $/MWh for the different cases. (a) No incentives, (b) EEC full access, (c) virtual machine.

Case	$T_{min} = 50^{\circ}C$	$T_{min} = 70^{\circ}C$
CO_2 MTR	66$^{(c)}$	31$^{(b)}$
$CO_2 + C_6F_6$ MTR	69$^{(c)}$	34$^{(b)}$
CO_2 MPP	76$^{(c)}$	39$^{(b)}$
$CO_2 + C_6F_6$ MPP	82$^{(c)}$	38$^{(b)}$
CO_2 MEE	74$^{(c)}$	38 $^{(b)}$
$CO_2 + C_6F_6$ MEE	76$^{(b)}$	37 $^{(b)}$
$CO_2 + C_6F_6$ SR	48$^{(b)}$	25 $^{(b)}$
Case 1	42$^{(a)}$	
Case 2 (actual CCHP)	27$^{(a)}$	
Case 3	39$^{(b)}$	
Case 4	23$^{(b)}$	

Fig. 15 illustrates the influence of natural gas prices and hot water selling prices for the three cases reported in Fig. 14. A decrease in natural gas prices has a positive impact on operational expenditure (OPEX), while a lower selling price for hot water implies a higher LCOE. In fact, a reduction in the natural gas price from $42/MWh to $35/MWh (−17 %) results in a reduction of more than 50 % in LCOE, depending on the configuration. Conversely, a reduction in the selling price of hot water (from $120/MWh to $80/MWh, –33 %) increases the LCOE by up to 48 % across case studies. Regarding uncertainties in capital expenditure for power cycle components, a 34 % reduction leads to an LCOE of $24/MWh and $34/MWh for pure (MTR) and mixture (MEE) CS configurations at a minimum temperature $T_{min} = 70^{\circ}C$, and $23/MWh for SR cycle at $T_{min} = 70^{\circ}C$. Meanwhile, at the same minimum cycle temperature, a 34 % increase in CAPEX for the cycle results in LCOEs of $36/MWh, $62/MWh, and $28/MWh for the three mentioned cycle configurations.

Two fundamental aspects which strongly influence the results of the proposed analysis: the geographical location of the plant and the price of natural gas. The first influences the number of operating hours of the various components of the trigeneration plant and consequently the potential economic gains. Colder climates clearly favour hot water

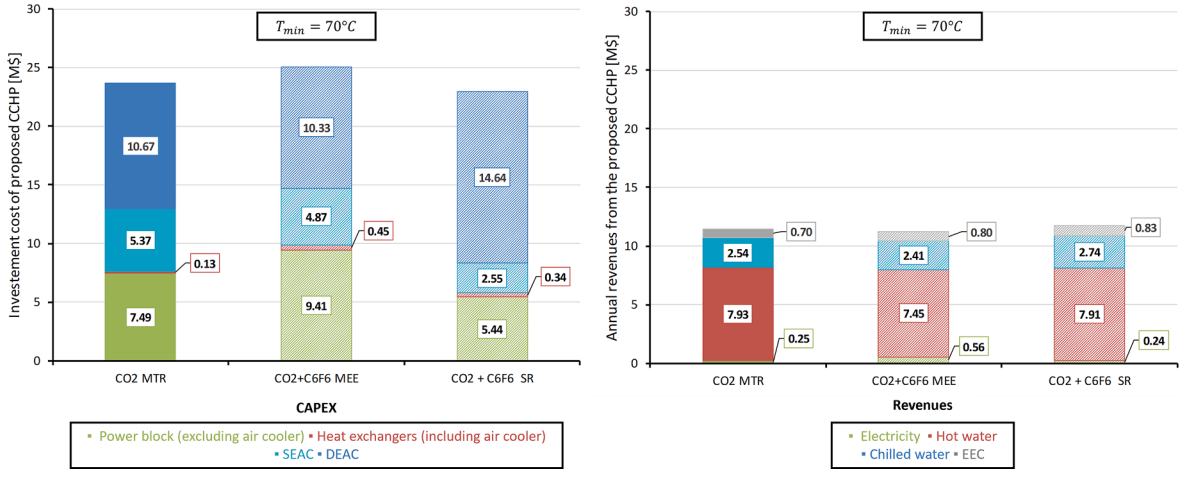

Fig. 14. CAPEX (left) and revenues (right) for the pure CO_2 MTR, blended CO_2 MEE and SR at $T_{min} = 70^{\circ}C$.

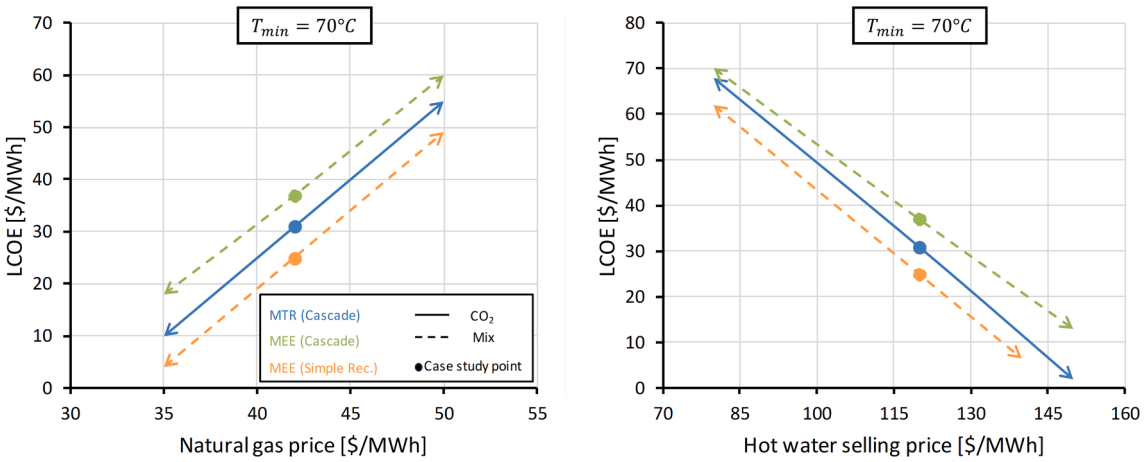

Fig. 15. Sensitivity analysis on natural gas price (left) and hot water selling price (right) for the most economical cases.

production for DH and warmer climates cold water production for the DC: in this specific case study, the operating hours for district heating are about five and a half months per year compared to only three months in summer for district cooling. In this analysis, hot water price is nearly double that of chilled water, and coupled with DH and DC operating hours, configurations favouring electricity production (e.g., MPP and low T_{min}) are most disadvantaged.

Based on the economic considerations, two cycle configurations looks promising for the investigated application. Among the cascade configuration, the MTR cycle is the most appropriate one being able of produce more thermal power that can be used in DH and DC network and thus increase the annual incomes. The other one is the SR cycle which presents almost the same LCOE whit a higher PES index and electric efficiency. Lastly, Table 9 shows the LCOE for the additional cases presented in section 2.5 too.

Case 1 and *Case 2* (the actual CCHP plant) presents a LCOE equal to 42 and 27 $/MWh with a PES that does not grant the access to EEC scheme, while the PES index for *Case 3* and *Case 4* is 10 % and 12 %. Due to the high DEACs CAPEX, standing at 34.4 M$, Case 3 has an LCOE equal to 39 $/MWh, in line with the MEE and MPP cascade at $T_{min} = 70^{\circ}C$. Nevertheless, the most advantageous economic solution is *Case 4* with a LCOE lower than the simple recuperative cycle value.

4. Conclusion

This study explores the trigenerative potential of pure CO_2 and CO_2-mixture power cycles for heat recovery. Initially, cold thermal power production for a district cooling network is modelled, considering two types of H_2O-LiBr absorption chillers and their COP under varying heat source conditions. Results serve as references for combined cooling, heating, and power plants.

Using pure CO_2 and CO_2 mixtures in small-scale applications offers electrical efficiency of up to 30 % and consistent thermal benefits. Unlike ORC technology, which often compromises electrical output for district heating needs, CO_2-based cycles supply useful heat even at minimum temperatures of 50 °C or 70 °C.

In a techno-economic study on revamping a northern Italy trigeneration plant, employing CO_2 and CO_2 mixture cycles as working fluids enhances electric power production by 15 % to 35 %, depending on minimum cycle temperature. Despite lower electricity production from maximizing thermal recovery, the MTR configuration presents a lower levelized cost of electricity due to increased income from district heating. Optimal matching between heat rejection, recovery units, and thermal users highlights absorption chillers as a solution for increased capacity and environmental sustainability. A simpler power block layout, like the simple recuperative cycle, improves electric efficiency (above 29 % even at low minimum cycle temperature), albeit with lower annual electric production, leading to advantages in economic analysis, primary energy savings (up to 18 %), and lower carbon emissions.

In conclusion, CO_2 and C_6F_6 mixture adoption is preferable from a techno-economic standpoint compared to pure CO_2 for electricity generation, particularly at high minimum cycle temperatures. Feasibility depends on factors like geographical location, natural gas prices, and incentives, with the optimal solution influenced by hot water prices and district heating running hours, favouring the simple recuperative cycle with CO_2 mixture for maximizing electric efficiency.

CRediT authorship contribution statement

Mattia Baiguini: Conceptualization, Investigation, Methodology, Software, Validation, Visualization, Writing – original draft, Writing – review & editing. **Michele Doninelli:** Conceptualization, Investigation, Methodology, Writing – original draft, Writing – review & editing. **Ettore Morosini:** Conceptualization, Investigation, Methodology, Writing – original draft, Writing – review & editing. **Dario Alfani:** Investigation, Software, Validation, Writing – review & editing. **Gioele Di Marcoberardino:** Conceptualization, Methodology, Investigation, Visualization, Writing – original draft, Writing – review & editing. **Paolo Giulio Iora:** Supervision, Writing – review & editing. **Giampaolo Manzolini:** Supervision, Writing – review & editing, Funding acquisition. **Costante Mario Invernizzi:** Supervision, Writing – review & editing. **Marco Astolfi:** Conceptualization, Investigation, Methodology, Supervision, Writing – original draft, Writing – review & editing.

Declaration of competing interest

The authors declare that they have no known competing financial interests or personal relationships that could have appeared to influence the work reported in this paper.

Data availability

Data will be made available on request.

Acknowledgement

This publication was produced while attending the PhD programme in PhD in Sustainable Development And Climate Change at the University School for Advanced Studies IUSS Pavia, Cycle XXXVIII, with the support of a scholarship financed by the Ministerial Decree no. 351 of 9th April 2022, based on the NRRP - funded by the European Union - NextGenerationEU. (web site phd-sdc.it).

This study was carried out within the NEST - Network 4 Energy Sustainable Transition (D.D. 1243 02/08/2022, PE00000021) and received funding under the National Recovery and Resilience Plan (NRRP), Mission 4 Component 2 Investment 1.3, funded from the European Union - NextGenerationEU. This manuscript reflects only the authors' views and opinions, neither the European Union nor the European Commission can be considered responsible for them.

Appendix A

In this appendix, the physical properties of the absorption chillers and power cycle mixtures are reported as well as the COP results for both SEAC and DEAC.

Table A1
Physical properties of water and lithium bromide.

	Water	Lithium Bromide
CAS number	7732–18-5	7550–35-8
Chemical formula	H_2O	LiBr
Molar weight, kg/kmol	18.01	86.85
Melting temperature at 1 atm, °C	0	547
Boiling temperature at 1 atm, °C	99.98	1265
Density at 25 °C and 1 atm, kg/m^3	1000	3460
Water solubility at 20 °C and 1 atm, kg/L	–	1.49

Table A2
Pure fluids and mixture properties. The correlation for the binary parameter is taken from [36].

Fluids	CAS number	Molar weight [kg/kmol]	T_{cr} [°C]	P_{cr} [bar]	Binary interaction parameter [-]
CO_2	124–38-9	44.01	31.06	73.83	$k_{ij} = 0.16297 - 0.0003951 \bullet T[K]$
C_6F_6	392–56-3	186.06	243.58	32.73	

Table A3
COP results for SEAC. Temperature and temperature differences are reported in °C.

ΔT_{HTF}	$T_{HTF,in}$								
	80	**85**	**90**	**95**	**100**	**105**	**110**	**115**	**120**
10	0.584	0.797	0.822	0.824	0.823	0.816	0.807	0.798	0.790
20	0.430	0.710	0.774	0.824	0.823	0.816	0.807	0.798	0.790
30	0.340	0.641	0.722	0.758	0.779	0.778	0.773	0.769	0.764
40	0.281	0.584	0.676	0.720	0.745	0.745	0.741	0.736	0.732
50	0.259	0.536	0.636	0.685	0.730	0.715	0.711	0.707	0.702

Table A4
COP results for DEAC. Temperature and temperature differences are reported in °C.

ΔT_{HTF}	$T_{HTF,in}$				
	120	**130**	**140**	**150**	**160**
10	1.415	1.434	1.497	1.493	1.4783
20	0.917	1.249	1.417	1.446	1.434
30	0.843	1.142	1.348	1.391	1.383
40	0.756	1.053	1.287	1.338	1.332
50	0.572	0.979	1.231	1.292	1.284

Table A5
Coefficients for the polynomial regression in Equation (5). Coefficients are valid for $10^\circ C < \Delta T_{hs} < 50^\circ C$.

	Single Effect		Double effect	
	$80^\circ C < T_{hs} < 95^\circ C$	$100^\circ C < T_{hs} < 120^\circ C$	$120^\circ C < T_{hs} < 135^\circ C$	$140^\circ C < T_{hs} < 160^\circ C$
a_{00}	−163.8	0.3295	3.343	1.301
a_{10}	5.468	0.01389	−0.01275	0.006097
a_{01}	−0.1615	0.009043	−0.5465	−0.187
a_{20}	−0.06037	−0.0001197	1.45E-05	−2.98E-05
a_{11}	0.002316	−0.0001299	0.005651	0.002211
a_{02}	0.001333	−0.0001832	0.004287	0.0003054

(continued on next page)

Table A5 (*continued*)

	Single Effect		Double effect	
	$80^{\circ}C < T_{hs} < 95^{\circ}C$	$100^{\circ}C < T_{hs} < 120^{\circ}C$	$120^{\circ}C < T_{hs} < 135^{\circ}C$	$140^{\circ}C < T_{hs} < 160^{\circ}C$
a_{30}	0.0002216	2.667E-07	0	0
a_{21}	−0.0000063	1.057E-06	−1.485E-05	−6.630E-06
a_{12}	−1.541E-05	−1.414E-06	−1.996E-05	−2.264E-06
a_{03}	8.958E-07	3.350E-06	−1.639E-05	5.194E-07

$$COP(T_{hs},\Delta T_{hs}) = a_{00} + a_{10}T_{hs} + a_{01}\Delta T_{hs} + a_{02}T_{hs}^2 + a_{11}T_{hs}\Delta T_{hs} + a_{02}\Delta T_{hs}^2 + a_{30}T_{hs}^3 + a_{21}T_{hs}^2\Delta T_{hs} + a_{12}T_{hs}\Delta T_{hs}^2 + a_{03}\Delta T_{hs}^3$$

Appendix B

In this section the step-by-step calculation for the economic analysis is presented. As mentioned the cost of the gas turbine is taken from [52] while the power block components cost are computed according to the correlation of Weiland et al [53] and the correlation of Wright et al [54] only for the gas-CO_2 PHE. These cost correlations are not reported in this work, however Table shows the costs of the SEAC, DEAC and compression chiller according to [56] and [59], already actualized to the years 2023.

Table B1
Specific CAPEX and OPEX for the adsorption and compression chillers actualized to the years 2023.

Components	Referenced size	Specific CAPEX	Specific OPEX
SEAC	1550 kW	915 $/kW	0.005c$/kW•y
DEAC	4650 kW	875 $/kW	0.002c$/kW•y
Compression chiller	2500 kW	76 $/kW	4600 $/y

The cost C_{2023} of each components is actualized with the Chemical Engineering Plant Cost Index (CEPCI) [60] as reported in Equation (E.1). The CEPCI value for the different references is reported in Table while the 2023 CEPCI is 793.5.

$$C_{2023} = C_i\frac{CEPCI_{2023}}{CEPCI_i} \tag{E.1}$$

Table B2
CEPCI for the CCHP components.

Components	Reference	Year	CEPCI	Additional notes
Gas turbine	Gas turbine world handbook [52]	2018	603.1	–
Power block (excluding PHE)	Weiland et al [53]	2019	607.5	–
Power block PHE	Wright et al [54]	2019	541.7	–
HRejU	Jaric et al [56]	2014	576.1	The correlation is the Equation (2) in Table 1 [56]
HRecU	Smith [59]	2000	394.3	Correlation based on the internal area

The total investment cost C_{TOT}(Equation (E.2)) is the contribution of the components CAPEX and the balance of plant which is the 20 % of the CAPEX.

$$C_{TOT} = 1.2\sum CAPEX_i \tag{E.2}$$

The analysis consists in the calculation of the LCOE that set to zero the net present value (NPV – Equation (E.3)) at the end of the lifetime (25 years) of the proposed CCHP plant.

$$NPV = C_{TOT} + \sum_{n=0}^{25}\frac{CF_n}{(1+dr)^n} = 0 \tag{E.3}$$

CF_n is the cash flow at the year n, and dr is the discount rate equal to 8 %. The cash flow (Equation (E.4)) is computed as follow:

$$CF_n = I_n - OPEX_{TOT,n} - T_n \tag{E.4}$$

$$I_n = LCOE \bullet E_{EE} + p_{DH}E_{DH} + p_{DC}E_{DC} + p_{EEC}EEC \tag{E.5}$$

$$EEC = 0.086\left(\frac{E_{DC}}{\eta_{gb,ref} \bullet COP_{ref}} + \frac{E_{EE}}{\eta_{grid} \bullet \eta_{EE,ref}} + \frac{E_{DH}}{\eta_{gb,ref}} - E_{CCHP,LHV}\right) \tag{E.6}$$

$$OPEX_{TOT,n} = OPEX_{cycle} + OPEX_{SEAC} + OPEX_{DEAC} + c_{NG}E_{CCHP} \tag{E.7}$$

$$Am_n = \frac{C_{inv,TOT}}{n_{am}} \tag{E.8}$$

$$T_n = t \cdot (I_n - OPEX_{TOT,n} - Am_n) \tag{E.9}$$

I_n is the annual income considering the selling of electricity, hot and chilled water, and the remuneration from EEC (Equation (E.5)). The number of EEC (Equation (E.6)) is expressed in tonnes of oil equivalent: 0.086 is a conversion factor. $OPEX_{TOT,n}$ are the total operative expensive comprehensive of power cycle, SEAC and DEAC OPEX and the cost due to the natural gas consumption (Equation (E.7)). Am_n is the amortisation (Equation (E.8) that last 10 year (n_{am}), while T_n is the annual taxation considering a tax rate t equal to 43 % (Equation (E.9)). All the CAPEX is allocated at the first year.

Appendix C. Supplementary data

Supplementary data to this article can be found online at https://doi.org/10.1016/j.applthermaleng.2024.123943.

References

[1] I. - International Energy Agency, "The Future of Cooling Opportunities for energy-efficient air conditioning Together Secure Sustainable", Accessed: Mar. 07, 2023. [Online]. Available: www.iea.org/t&c/.

[2] IEA, "Heating," 2022. Accessed: Mar. 07, 2023. [Online]. Available: https://www.iea.org/reports/heating.

[3] M. Krarti, "Optimal design and retrofit of energy efficient buildings, communities, and urban centers," *Optim. Des. Retrofit Energy Effic. Build. Communities, Urban Centers*, pp. 1–625, Mar. 2018, doi: 10.1016/C2016-0-02074-0.

[4] C. M. Invernizzi, "Closed power cycles : thermodynamic fundamentals and applications," 2013, Accessed: Feb. 10, 2022. [Online]. Available: https://books.google.com/books/about/Closed_Power_Cycles.html?hl=it&id=RV9DAAAAQBAJ.

[5] G. Lozza, "Turbine a gas e cicli combinati. Seconda edizione," pp. 1–200, 2023, Accessed: Aug. 01, 2023. [Online]. Available: https://re.public.polimi.it/handle/11311/263873.

[6] "AIRU-the Italian District Heating Association-promotes and spreads the application and innovation of energy installations in district heating systems." [Online]. Available: www.ecoline.it.

[7] M. Doninelli, G. Di Marcoberardino, P. Iora, M. Gelfi, C. M. Invernizzi, and G. Manzolini, "Silicon Tetrachloride as innovative working fluid for high temperature rankine cycles: Thermal Stability, material compatibility, and energy analysis," *Appl. Therm. Eng.*, p. 123239, Apr. 2024, doi: 10.1016/J.APPLTHERMALENG.2024.123239.

[8] E. Macchi and M. Astolfi, *Organic Rankine Cycle (ORC) Power Systems - 1st Edition*, 1st Editio. 2017. doi: https://doi.org/10.1016/C2014-0-04239-6.

[9] M.J. Li, H.H. Zhu, J.Q. Guo, K. Wang, W.Q. Tao, The development technology and applications of supercritical CO2 power cycle in nuclear energy, solar energy and other energy industries, Appl. Therm. Eng. 126 (Nov. 2017) 255–275, https://doi.org/10.1016/J.APPLTHERMALENG.2017.07.173.

[10] E. Morosini, A. Ayub, G. di Marcoberardino, C.M. Invernizzi, P. Iora, G. Manzolini, Adoption of the CO2 + SO2 mixture as working fluid for transcritical cycles: A thermodynamic assessment with optimized equation of state, Energy Convers. Manag. 255 (Mar. 2022) 115263, https://doi.org/10.1016/J.ENCONMAN.2022.115263.

[11] M. Doninelli *et al.*, "Experimental investigation of the CO2+SiCl4 mixture as innovative working fluid for power cycles: Bubble points and liquid density measurements," *Energy*, p. 131197, Apr. 2024, doi: 10.1016/J.ENERGY.2024.131197.

[12] M. Astolfi, D. Alfani, S. Lasala, E. Macchi, Comparison between ORC and CO2 power systems for the exploitation of low-medium temperature heat sources, Energy 161 (Oct. 2018) 1250–1261, https://doi.org/10.1016/J.ENERGY.2018.07.099.

[13] A. Huicochea, W. Rivera, G. Gutiérrez-Urueta, J.C. Bruno, A. Coronas, Thermodynamic analysis of a trigeneration system consisting of a micro gas turbine and a double effect absorption chiller, Appl. Therm. Eng. 31 (16) (Nov. 2011) 3347–3353, https://doi.org/10.1016/J.APPLTHERMALENG.2011.06.016.

[14] H. Jaubert, P. Borel, P. Guichardon, J.F. Portha, J.N. Jaubert, L. Coniglio, Assessment of organic Rankine cycle configurations for solar polygeneration orientated to electricity production and desalination, Appl. Therm. Eng. 195 (Aug. 2021) 116983, https://doi.org/10.1016/J.APPLTHERMALENG.2021.116983.

[15] A. Kasaeian, M. Javidmehr, M.R. Mirzaie, L. Fereidooni, Integration of solid oxide fuel cells with solar energy systems: A review, Appl. Therm. Eng. 224 (Apr. 2023) 120117, https://doi.org/10.1016/J.APPLTHERMALENG.2023.120117.

[16] E. Bellos, Z. Said, P. Lykas, C. Tzivanidis, A review of polygeneration systems with CO2 working fluid, Therm. Sci. Eng. Prog. 34 (2022) 101435, https://doi.org/10.1016/j.tsep.2022.101435.

[17] L. Moroz, M. Burlaka, and O. Rudenko, "Study of a Supercritical CO2 Power Cycle Application in a Cogeneration Power Plant".

[18] S. Chen, A. Soomro, R. Yu, J. Hu, Z. Sun, W. Xiang, Integration of chemical looping combustion and supercritical CO2 cycle for combined heat and power generation with CO2 capture, Energy Convers. Manag. 167 (Jul. 2018) 113–124, https://doi.org/10.1016/J.ENCONMAN.2018.04.083.

[19] Y. Yang, Y. Huang, P. Jiang, Y. Zhu, Multi-objective optimization of combined cooling, heating, and power systems with supercritical CO2 recompression Brayton cycle, Appl. Energy 271 (Aug. 2020) 115189, https://doi.org/10.1016/J.APENERGY.2020.115189.

[20] J. Zhang, J. Wang, W. Liu, B. Hu, J. Lou, P. Zhao, Multi-objective optimization design of a solar-powered integrated multi-generation system based on combined SCO2 Brayton cycle and ORC using machine learning approach, Appl. Therm. Eng. 252 (Sep. 2024) 123684, https://doi.org/10.1016/J.APPLTHERMALENG.2024.123684.

[21] E. Morosini, M. Doninelli, D. Alfani, M. Astolfi, G. Di Marcoberardino, and G. Manzolini, "Analysis of the potential of CO2 based mixtures to improve the efficiency of cogenerative waste heat recovery power plants," *5th Eur. sCO2 Conf. Energy Syst. March 14-16, 2023, Prague, Czech Repub.*, pp. 169–178, Apr. 2023, doi: 10.17185/DUEPUBLICO/77287.

[22] D. Alfani, M. Binotti, E. Macchi, P. Silva, M. Astolfi, sCO2 power plants for waste heat recovery: design optimization and part-load operation strategies, Appl. Therm. Eng. 195 (Aug. 2021) 117013, https://doi.org/10.1016/J.APPLTHERMALENG.2021.117013.

[23] M. Doninelli, et al., Thermal desalination from rejected heat of power cycles working with CO2-based working fluids in CSP application: A focus on the MED technology, Sustain. Energy Technol. Assessments 60 (Dec. 2023) 103481, https://doi.org/10.1016/J.SETA.2023.103481.

[24] "Aspen Plus | Leading Process Simulation Software | AspenTech." https://www.aspentech.com/en/products/engineering/aspen-plus (accessed Apr. 11, 2023).

[25] A2a,, L'impianto di cogenerazione di Milano | A2A, (accessed Mar. 07 (2023) 2023). https://www.gruppoa2a.it/it/chi-siamo/nostri-impianti/teleriscaldamento/milano-tecnocity.

[26] Solar Turbines, "Taurus 60," 2023. https://www.solarturbines.com/en_US/products/gas-compressor-packages/taurus-60.html (accessed Mar. 07, 2023).

[27] MISE, "Progetto modifica della Centrale di teleriscaldamento di Milano Bicocca, localizzata nel Comune di Milano - Info - Valutazioni e Autorizzazioni Ambientali - VAS - VIA - AIA," 2020. https://va.mite.gov.it/it-IT/Oggetti/Info/7576 (accessed Mar. 07, 2023).

[28] F. Crespi, G. Gavagnin, D. Sánchez, G.S. Martínez, Supercritical carbon dioxide cycles for power generation: A review, Appl. Energy 195 (Jun. 2017) 152–183, https://doi.org/10.1016/J.APENERGY.2017.02.048.

[29] G. Manzolini, M. Binotti, D. Bonalumi, C. Invernizzi, P. Iora, CO2 mixtures as innovative working fluid in power cycles applied to solar plants. Techno-economic assessment, Sol. Energy 181 (Mar. 2019) 530–544, https://doi.org/10.1016/J.SOLENER.2019.01.015.

[30] M. Doninelli and G. Di Marcoberardino, "On the Design of Recuperator for Transcritical Cycle Adopting CO2-Based Mixture as Working Fluid: A Focus on Transport Properties Prediction," *Energy Technol.*, p. 2300677, 2023, doi: 10.1002/ENTE.202300677.

[31] "(13) (PDF) Binary mixtures of carbon dioxide and fluorocarbons: review of thermodynamic data and their modelling." https://www.researchgate.net/publication/346571044_Binary_mixtures_of_carbon_dioxide_and_fluorocarbons_review_of_thermodynamic_data_and_their_modelling (accessed Apr. 20, 2024).

[32] S. Lasala, D. Bonalumi, E. Macchi, R. Privat, J.N. Jaubert, The design of CO2-based working fluids for high-temperature heat source power cycles, Energy Procedia 129 (Sep. 2017) 947–954, https://doi.org/10.1016/J.EGYPRO.2017.09.125.

[33] E. Morosini, et al., Off-design of a CO2-based mixture transcritical cycle for CSP applications: Analysis at part load and variable ambient temperature, Appl. Therm. Eng. 236 (Jan. 2024) 121735, https://doi.org/10.1016/J.APPLTHERMALENG.2023.121735.

[34] P. Rodríguez-deArriba, F. Crespi, D. Sánchez, A. Muñoz, T. Sánchez, The potential of transcritical cycles based on CO2 mixtures: An exergy-based analysis, Renew. Energy 199 (Nov. 2022) 1606–1628, https://doi.org/10.1016/J.RENENE.2022.09.041.

[35] E. Morosini, E. Villa, G. Quadrio, M. Binotti, G. Manzolini, Solar tower CSP plants with transcritical cycles based on CO2 mixtures: A sensitivity on storage and power block layouts, Sol. Energy 262 (Sep. 2023) 111777, https://doi.org/10.1016/J.SOLENER.2023.05.054.

[36] G. Di Marcoberardino, et al., Experimental characterisation of CO2 + C6F6 mixture: thermal stability and vapour liquid equilibrium test for its application in transcritical power cycle, Appl. Therm. Eng. (2022) 118520, https://doi.org/10.1016/j.applthermaleng.2022.118520.

[37] V. Illyés *et al.*, "sCO2 test facility at TU Wien: design, operation and results," *5th Eur. sCO2 Conf. Energy Syst. March 14-16, 2023, Prague, Czech Repub.*, pp. 22–37, Apr. 2023, doi: 10.17185/DUEPUBLICO/77261.
[38] R. Span, W. Wagner, A new equation of state for carbon dioxide covering the fluid region from the triple-point temperature to 1100 K at pressures up to 800 MPa, J. Phys. Chem. Ref. Data 25 (6) (1996) 1509–1596, https://doi.org/10.1063/1.555991.
[39] C. W. White and N. T. Weiland, "Evaluation of Property Methods for Modeling Direct-Supercritical CO2 Power Cycles," *J. Eng. Gas Turbines Power*, vol. 140, no. 1, Jan. 2018, doi: 10.1115/1.4037665/374499.
[40] M. Doninelli, G. Di Marcoberardino, C.M. Invernizzi, P. Iora, Experimental isochoric apparatus for bubble points determination: Application to CO_2 binary mixtures as advanced working fluids, Int. J. Thermofluids 23 (2024) 100742, https://doi.org/10.1016/j.ijft.2024.100742.
[41] S.I. Salah, et al., Axial turbine flow path design for concentrated solar power plants operating with CO2 blends, Appl. Therm. Eng. 230 (Jul. 2023) 120612, https://doi.org/10.1016/J.APPLTHERMALENG.2023.120612.
[42] C. Somers, A. Mortazavi, Y. Hwang, R. Radermacher, P. Rodgers, S. Al-Hashimi, Modeling water/lithium bromide absorption chillers in ASPEN Plus, Appl. Energy 88 (11) (Nov. 2011) 4197–4205, https://doi.org/10.1016/J.APENERGY.2011.05.018.
[43] K. E. Herold, R. Radermacher, and S. A. Klein, *Absorption chillers and heat pumps*. Accessed: Dec. 11, 2023. [Online]. Available: https://www.routledge.com/Absorption-Chillers-and-Heat-Pumps/Herold-Radermacher-Klein/p/book/9781498714341.
[44] S. M. Osta-Omar and C. Micallef, "Mathematical Model of a Lithium-Bromide/Water Absorption Refrigeration System Equipped with an Adiabatic Absorber," *Comput. 2016, Vol. 4, Page 44*, vol. 4, no. 4, p. 44, Nov. 2016, doi: 10.3390/COMPUTATION4040044.
[45] L. G. Farshi, S. M. Seyed Mahmoudi, M. A. Rosen, and M. Yari, "Use of low grade heat sources in combined ejector-double effect absorption refrigeration systems," 2012, doi: 10.1177/0957650912446902.
[46] S. Salehi, M. Yari, S.M.S. Mahmoudi, L.G. Farshi, Investigation of crystallization risk in different types of absorption LiBr/H2O heat transformers, Therm. Sci. Eng. Prog. 10 (May 2019) 48–58, https://doi.org/10.1016/J.TSEP.2019.01.013.
[47] "Greenhouse gas emission intensity of electricity generation in Europe — European Environment Agency."." https://www.eea.europa.eu/ims/greenhouse-gas-emission-intensity-of-1 (accessed Sep. 20, 2023).
[48] F.W. Yu, K.T. Chan, R.K.Y. Sit, J. Yang, Review of Standards for Energy Performance of Chiller Systems Serving Commercial Buildings, Energy Procedia 61 (Jan. 2014) 2778–2782, https://doi.org/10.1016/J.EGYPRO.2014.12.308.
[49] "Summary of Abundances, Lifetimes, ODPs, REs, GWPs, and GTPs." https://tsapps.nist.gov/publication/get_pdf.cfm?pub_id=936562 (accessed Apr. 20, 2024).
[50] "EUR-Lex - 32015R2402 - EN - EUR-Lex." https://eur-lex.europa.eu/legal-content/EN/ALL/?uri=CELEX%3A32015R2402 (accessed Dec. 11, 2023).
[51] "Gazzetta Ufficiale." https://www.gazzettaufficiale.it/eli/id/2011/09/19/11A12047/sg (accessed Jan. 31, 2024).
[52] "2018 Handbook, Volume 33 - Gas Turbine World." https://gasturbineworld.com/shop/annual-handbook/2018-handbook-volume-33/ (accessed Jan. 22, 2024).
[53] N. T. Weiland, B. W. Lance, and S. R. Pidaparti, "SCO2 power cycle component cost correlations from DOE data spanning multiple scales and applications," in *Proceedings of the ASME Turbo Expo*, American Society of Mechanical Engineers (ASME), 2019. doi: 10.1115/GT2019-90493.
[54] S. Wright, … C. D.-F. I. S., and undefined 2016, "Thermo-economic analysis of four sCO2 waste heat recovery power systems," *sco2symposium.com*, 2016, Accessed: Apr. 05, 2023. [Online]. Available: http://sco2symposium.com/papers2016/SystemModeling/059paper.pdf.
[55] M. Marchionni, G. Bianchi, S.A. Tassou, Techno-economic assessment of Joule-Brayton cycle architectures for heat to power conversion from high-grade heat sources using CO2 in the supercritical state, Energy 148 (Apr. 2018) 1140–1152, https://doi.org/10.1016/J.ENERGY.2018.02.005.
[56] U. States Department of Energy, "Combined Heat and Power Technology Fact Sheet Series ADVANCED MANUFACTURING OFFICE".
[57] M. Jarić, M. Dobrnjac, N. Budimir, and T. Bajc, "COST ANALYSIS OF SHELL AND TUBE HEAT EXCHANGERS WITH CONCENTRIC HELICAL TUBE COILS," *Proc. / 6th Int. Symp. Ind. Eng. - SIE 2015, 24th-25th Sept. 2015, Belgrade*, pp. 195–199, 2015, Accessed: Jan. 22, 2024. [Online]. Available: https://machinery.mas.bg.ac.rs/handle/123456789/4398.
[58] R. Smith, "Chapter 2 - Process Economics," *Chem. Process Des. Integr.*, p. 21, 2016, Accessed: Jan. 22, 2024. [Online]. Available: https://www.wiley.com/en-us/Chemical+Process+Design+and+Integration%2C+2nd+Edition-p-9781119990147.
[59] ASHRAE, "2013 ASHRAE Handbook - Fundamentals (SI Edition)," *2013 ASHRAE Handbook—Fundamentals*, vol. 2013, no. 38, pp. 15.18-15.36, 2013.
[60] "Cost Indices – Towering Skills." https://toweringskills.com/financial-analysis/cost-indices/ (accessed Dec. 26, 2023).